1

The Velardeña Zn–(Pb–Cu) skarn-epithermal deposits, central-northern Mexico: New physical-chemical constraints on ore-forming processes

El sistema skarn-epitermal de Zn–(Pb–Cu) de Velardeña, Durango (México): Nuevos datos fisicoquímicos de los procesos de mineralización

Abigail **Jiménez-Franco**[1,2,3*], Carles **Canet**[4,5], Pura **Alfonso**[6], Eduardo **González-Partida**[7], Abdorrahman **Rajabi**[8], Edgar **Escalante**[9]

[1] Departament de Mineralogia, Petrologia i Geologia Aplicada, Universitat de Barcelona, Marti i Franquès s/n, 08028, Barcelona, Catalunya, Spain.

[2] Institut de Nanociència i Nanotecnologia, IN2UB Facultat de Química, Universitat de 8 Barcelona, Av. Diagonal 645, 08028 Barcelona, Catalunya, Spain.

[3] Posgrado en Ciencias de la Tierra, Universidad Nacional Autónoma de México, Ciudad Universitaria, Coyoacán, 04510, CDMX, Mexico.

[4] Centro de Ciencias de la Atmósfera, Universidad Nacional Autónoma de México, Ciudad Universitaria, Coyoacán, 04510, CDMX, Mexico.

[5] Instituto de Geofísica, Universidad Nacional Autónoma de México, Ciudad Universitaria, Coyoacán, 04510, CDMX, Mexico.

[6] Dept. d'Enginyeria Minera, Industrial i TIC, Universitat Politècnica de Catalunya, Av. de les Bases de Manresa 61-73, 08242 Manresa, Barcelona, Spain.

[7] Centro de Geociencias, Universidad Nacional Autónoma de México, Campus Juriquilla, 76230, Santiago de Querétaro, Mexico.

[8] School of Geology, College of Science, University of Tehran, 16th Azar St., Enghelab Sq., Tehran, Iran.

[8] Industrias Peñoles, prolongación Comonfort s/n, Col. Metalurgica, 27370, Torreón, Coahuila, Mexico.

* Corresponding author: (A. Jiménez-Franco)
abyjimenez@ub.edu

ABSTRACT

The Velardeña mining district is economically the most important of Durango state. The ore deposits occur in different skarn zones developed within the intrusive contact between Mesozoic limestones and Eocene granitic stocks and dikes. The most important ore deposits are related to the Santa María dike and Reyna de Cobre porphyritic stock (separated from each other by 10 km). They occur as irregularly shaped replacement masses developed near the intrusive contact and have a skarn paragenesis dominated by calc-silicates and sulfides. The mineral assemblages show replacement textures and are dominated by calcic clinopyroxene ($Di_{97-53}Hd_{42-02}Jh_{04-01}$) and garnet ($Ad_{100-57}Grs_{43-00}$) in the exoskarn, with wollastonite particularly abundant in the endoskarn. Hydrous silicates are actinolite, epidote, and chlorite, whereas sulfides include pyrite, sphalerite, pyrrhotite, galena, chalcopyrite, and sulfosalts. Scheelite, hematite, quartz, and calcite are also present. According to sphalerite geobarometry, the skarns formed at hypabyssal depths (~3–4 km). They developed by a succession of replacive mineralizing events, including (a) a prograde stage at temperatures from ≥470 to 335 °C in conditions of low f (CO_2), followed by (b) a retrograde stage from 335 to 220 °C. There was a general increase in f (O_2), accompanying the temperature decline during the formation of the system, which accounts for a process of mixing with cooler, oxidizing, and dilute water. During the retrograde stage, wollastonite, calcic garnet and clinopyroxene formed. On the other hand, hydrous silicates, sulfides, sulfosalts, scheelite, and hematite crystallized during the retrograde stage. Skarn mineralization is crosscut by veins of calcite, fluorite, adularia, and sphalerite. The vein mineralization formed at temperatures below 200 °C. The different ore deposits of Velardeña constitute a telescoped skarn–epithermal mineral system.

Keywords: paragenesis, geothermometry, epithermal–skarn telescoping, geochemical modeling, massive sulfides.

RESUMEN

El distrito minero Velardeña es económicamente el más importante del estado de Durango. En él, las mineralizaciones comprenden diferentes zonas de skarn, desarrolladas entre el contacto de calizas mesozoicas, stocks y diques del Eoceno. Los depósitos de Velardeña más importantes están relacionados al dique Santa María, y el stock porfídico Reyna de Cobre (separados entre sí ~10 km). La mineralización ocurre como reemplazamiento, formando cuerpos irregulares cerca del contacto con los intrusivos, caracterizados por una paragénesis típica de skarn (calcisilicatos y sulfuros). Las asociaciones minerales muestran texturas de reemplazo dominados por clinopiroxeno cálcico ($Di_{97-53}Hd4_{2-02}Jh_{04-01}$) y granate ($Ad_{100-57}Grs_{43-00}$) en el exoskarn, y wollastonita particularmente abundante en el endoskarn. Los hidrosilicatos son actinolita, epidota y clorita; los sulfuros incluyen pirita, esfalerita, pirrotita, galena, calcopirita y sulfosales. Scheelita, hematita, cuarzo y calcita también están presentes. El geobarómetro de esfalerita estima que las mineralizaciones tipo skarn de Velardeña se formaron a profundidades hipabisales (~ 3-4 km). La mineralización metálica se desarrolló por una sucesión de eventos de reemplazamiento, que incluyen (a) una etapa prógrada a ≥470 a 335 °C y baja $f(CO_2)$, seguida por (b) la etapa retrógrada de 335 a 220 °C. Hubo un aumento general de $f(O_2)$, durante el descenso de temperatura en la formación del yacimiento, debido a la mezcla de fluidos mineralizantes con agua más fría, oxidante y diluida. Durante la etapa retrógrada, se formaron wollastonita, granate cálcico y clinopiroxeno. La etapa prógrada dio lugar a la formación de hidrosilicatos, sulfuros (incluyendo sulfosales), scheelita y hematita. Además de las mineralizaciones tipo skarn en Velardeña, hay vetas epitermales de calcita, fluorita, adularia y esfalerita, cortando los calcosilicatos. La mineralización en estas vetas se estima que se formó a <200 °C. Por ello, es plausible proponer que los depósitos minerales que conforman el distrito minero Velardeña constituyen un sistema skarn-epitermal telescópeado.

Palabras clave: paragénesis, geotermometría, telescopeo skarn-epitermal, modelización geoquímica, sulfuros masivos.
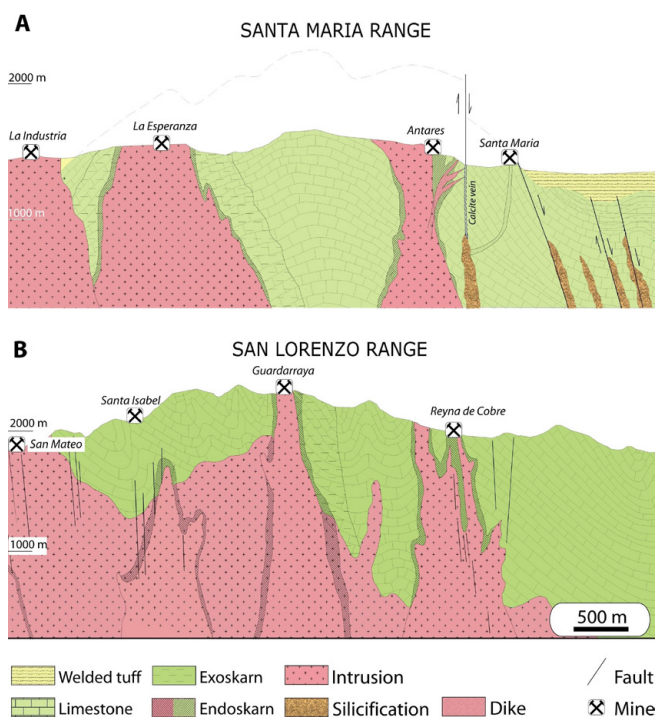
1. Introduction

Mesozoic carbonate rocks are widely distributed throughout central-northern and eastern Mexico, and in many places they were intruded by felsic to intermediate plutonic and hypabyssal rocks of Eocene age. As a result, numerous skarn deposits were formed through a complex succession of metallogenic stages (Camprubí, 2009). Some of these skarns are giant base-metal deposits, such as the Naica Zn–Pb(–Cu–Au–Ag) deposit in Chihuahua state (processing capacity: 690,000 t/yr of run-of-mine (ROM) ore Industrias Peñoles, 2016), the Concepción del Oro Cu(–Pb–Zn–Au) deposit (936000 t/yr ROM ore; SGM, 2014) and the Francisco I. Madero Zn–Cu–Pb(–Ag) deposit (2200000 t/yr ROM ore; Industrias Peñoles, 2016), both in Zacatecas state, and the Charcas Zn–Cu (–Ag–Pb) deposit in San Luis Potosí state (1460000 t/yr ROM ore; Southern Copper Corporation, 2016).

Another large ore deposit of this type is that of the Velardeña Pb–Zn(–Cu) mining district in central-northern Mexico, economically the most important district of Durango state. Felder (1979) calculated a total of 24 Mt of ore reserves for only one of the mineralized areas in Velardeña, the Santa María mine (Figure 1). This mine was the only productive one in the entire district in the 1970s and, after a three-decade interruption of mining activities, Industrias Peñoles resumed exploration in 2006. Due to its economic and geological interest, several works have been focused on the skarn mineralization of the Santa María mine, notably the metallogenic evolution (Spurr and Garrey, 1908; Levich, 1973; Gilmer *et al.*, 1986, 1988; Gilmer, 1987a, 1987b) and structural geology perspectives (Pinet and Tremblay, 2009).

However, the reactivation of exploration carried out in 2006 revealed new areas with economic potential in the northwest of the district, mainly at Reyna de Cobre (Figure 1).
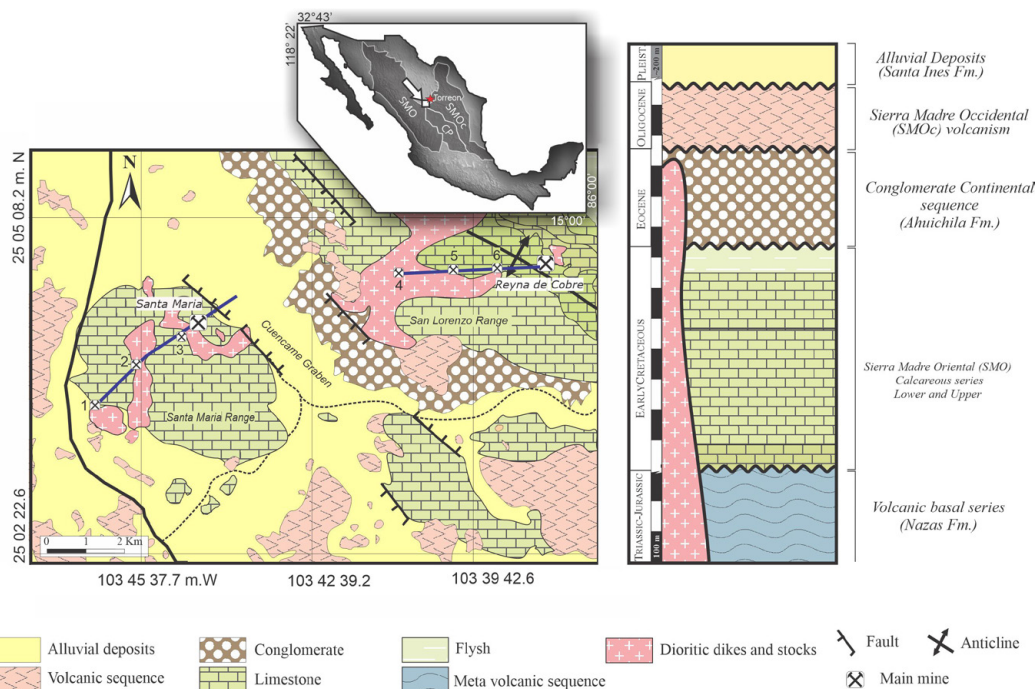
Figure 1 Location and detailed geological map of the Velardeña mining district, showing the two main ore deposits: Santa María and Reyna de Cobre. Minor ore occurrences are (1) La Industria, (2) La Esperanza, (3) Antares, (4) San Mateo, (5) Santa Isabel, and (6) Guardarraya. The schematic stratigraphic column (right) is based on SGM (1997). Geological schematic cross-sections of the Santa María (from La Industria to Santa María) and San Lorenzo (from San Mateo to Reyna del Cobre) ranges are shown in Figure 2. The top map shows the location of the Velardeña mining district in relation to the three main geological provinces of central-northern Mexico (Key: SMO = Sierra Madre Oriental; SMOc = Sierra Madre Occidental; CP = Central Plateau).

A

SANTA MARIA RANGE

B

SAN LORENZO RANGE

	Welded tuff		Exoskarn		Intrusion	/	Fault
	Limestone		Endoskarn		Silicification	☒	Mine
					Dike		

Figure 2   Schematic geological sections of the Velardeña mining district, with the location of the main ore deposits and occurrences. The location of both profiles is shown in Figure 1.

The Santa María and Reyna de Cobre mineralized areas are separated from each other by ~10 km, lying in the ranges of Santa María (to the west) and San Lorenzo (to the east), respectively (Figure 2). These two ranges are NW-trending anticlines dissected by a ~3 km wide graben filled by Eocene volcanic deposits and Quaternary sediments (Pinet and Tremblay, 2009).

This contribution presents new mineralogical (paragenesis and mineral chemistry), fluid inclusion (microthermometry), and geochemical (sulfur isotopes) data from the Velardeña mining district. The aim of this work is to elucidate the processes that led to the formation of skarns in the Velardeña mining district and to constrain the physical-chemical variables associated with these processes, such as temperature, pressure, f (CO_2), and f (O_2). In addition, the metallogenic connection between Reyna de Cobre and Santa María mineralized areas is analyzed and re-interpreted.

2. Geological setting

The Velardeña mining district is located in Durango state, ~60 km southwest of the city of Torreón. The mining district encompasses a 3 to 4 km wide, NW–SE trending graben, known as Cuencamé valley (Valle de Cuencamé), which is bounded by two mountain ranges: Santa María to the southwest and San Lorenzo to the northeast (Figures 1 and 2). All are developed along the intrusive contact between the Mesozoic limestones and the Eocene granitic stocks and dikes. Two intrusive bodies show a spatial association with the skarns of the Velardeña mining district, namely (*a*) the Antares dike (strike direction: NW–SE), located in the Santa María range (Figure 2a); and (*b*) the Reyna de Cobre porphyritic stock, in the San Lorenzo range (Figure 2b).

2.1. REGIONAL FRAMEWORK

The study area is situated at the junction of three physiographic provinces (Figure 1): (*a*) the Sierra Madre Oriental (SMO), (*b*) the Sierra Madre Occidental (SMOc), and (*c*) the Mesa Central (or Central Plateau, CP) (Figure 1). The SMO is a fold-and-thrust belt that resulted from the deformation of Mesozoic sedimentary rocks by the Laramide orogenesis in late Eocene times (Eguiluz-De-Antuñano *et al.*, 2000). On the other hand, the SMOc is a silicic volcanic arc resulting from the subduction of the former Farallon plate beneath North America, and it consists of a thick sequence of volcanic rocks, mostly andesites, rhyolites, and ignimbrites, with ages ranging from Upper Cretaceous to Eocene (*e.g.*, Ferrari *et al.*,2005).

The CP is an elevated plateau, with an average altitude of about 2000 m, bounded to the north and east by the SMO, to the west by the SMOc, and to the south by the E–W El Bajío Fault (Nieto-Samaniego *et al.*, 2005). Both the SMOc and the CP are richly endowed with ore deposits, particularly of precious and base metals (Damon *et al.*, 1981; Clark *et al.*, 1982; Camprubí, 2009). According to

Nieto-Samaniego *et al.* (2005), mineral deposits from the CP and in its vicinities are associated with major fault systems, which also control the emplacement of volcanic and hypabyssal rocks.

2.2. GEOLOGY OF THE STUDY AREA

The rocks of the study area correspond mainly to a predominantly carbonate transgressive Cretaceous sequence related to the opening of the Gulf of Mexico. This sequence was deposited unconformably on the meta-volcanosedimentary Nazas Formation, Upper Triassic to Lower Jurassic in age (SGM, 1997) (Figure 1). This unit, which does not crop out in the study area, consists of intermediate to silicic tuffs and lavas associated with red beds and affected by low-grade metamorphism, and it is crosscut by dikes of basaltic to andesitic composition (Barboza-Gudiño *et al.*, 2004). The rocks of the Nazas Formation represent a continental volcanic arc, developed from the Upper Triassic to the Lower Jurassic at the western margin of North America (Barboza-Gudiño *et al.*, 1998).

The Cretaceous transgressive sequence is represented in the study area by three formations: from the base to the top (Kelly, 1936; SGM 1997), (*a*) the Aurora Formation (Albian), with a thicness of 300–400 m, composed of thin-layered limestones rich in chert nodules; (*b*) the Cuesta del Cura Formation (Albian–Cenomanian), ~300 m in thickness, consisting of interbedded limestone and lutite; and (*c*) the Indidura Formation (Turonian), ~80 m in thickness, a flysch rhythmic alternation of mudstone and organic-matter-rich lutite beds. This sequence is unconformably overlain by the Ahuichila Formation (Eocene), with an average thickness of ~450 m, and which consists of continental conglomerates with carbonate cement and clasts coming from the underlying Cretaceous sequence (Rogers *et al.*, 1961).

Magmatic activity started in the Oligocene and continued through the Miocene, producing welded rhyolitic tuffs followed by andesitic and basaltic lavas (SGM, 1997). The rhyolitic tuffs form a ~160 m thick succession that fills the Cuencamé graben

and are covered by up to 300 m of Quaternary alluvial sediments (Figure 1). Eocene magmatism also produced felsic to intermediate (granitic to dioritic) hypabyssal stocks and NW–SE-trending dikes that crosscut the entire Mesozoic sequence and the Eocene Ahuichila conglomerates (Figures 1 and 2). Spurr and Garrey (1908) first noticed the relationship between ore mineralization and hypabyssal rocks in the Velardeña mining district.

These authors described the intrusive bodies and labeled them as "alaskites" and trachytes. A K-Ar age of 33.4 ±1.7 Ma (ca. Eocene–Oligocene boundary) was determined for magmatic biotite of the hypabyssal rocks associated with the ore mineralization in the Velardeña mining district by Felder (1979). As a whole, this district has been interpreted as a large volcano-plutonic complex that resulted from the overlapping of the SMOc arc magmatism and the Basin and Range extension (Levich, 1973; Gilmer *et al.*, 1986; Gilmer *et al.*, 1988). Due to the thick pyroclastic deposits accumulated in the Cuencamé graben (among other facts), Aguirre-Díaz *et al.* (2008) suggested the occurrence of a "graben-type caldera" volcanic center.

2.3. SKARNS IN THE VELARDEÑA MINING DISTRICT

The Santa María mine has been studied by several authors as a notable example of Zn–Pb skarn deposits (Spurr and Garrey, 1908; Ambriz, 1979; Levich, 1973; Gilmer *et al.*, 1986, 1988). Reyna de Cobre is also a skarn with mainly Pb-Zn mineralization, despite its name ("Copper Queen" in Spanish), which comes from the striking blue-green secondary copper minerals that occur on the surface. In both areas, the mineralization is associated with intrusive contact of dikes and stocks with the calcareous strata and, occurs (*a*) as irregularly shaped replacement masses with a paragenesis dominated by calc-silicates and sulfides, and (*b*) as high-grade calcite–fluorite–sphalerite (–adularia, –quartz) veins placed in the skarn sequence.

The ore deposit-related igneous rocks of the Velardeña mining district have been petrographically classified as monzogranites with porphyritic

to granular textures (Jiménez-Franco, 2012). They contain subhedral phenocrysts, up to 4 mm in length, consisting of quartz and K-feldspar with subordinate plagioclase and biotite. K-feldspar usually appears partly altered to sericite. A few meters away from the contact with the carbonate rock, an endoskarn zone is developed on the intrusive bodies, showing pervasive silicification with wollastonite, epidote, chlorite and calcite, and disseminated pyrite, chalcopyrite and sphalerite.

The exoskarn is irregular in shape and thickness, up to 50 m; it consists of a calc-silicate-rich assemblage, variable in grain size, with replacive, inequigranular texture, and contains the volumetrically higher sulfide mineralization. The predominant calc-silicates are calcic garnet and clinopyroxene (plus subordinate wollastonite), garnet being the most abundant, and are accompanied by a later assemblage of calcic amphibole, chlorite, calcite and quartz with associated sulfides. The sulfides are principally sphalerite (marmatite variety), galena and chalcopyrite, with abundant pyrite and pyrrhotite, and occur (*a*) as massive, centimeter-sized, coarse-grained aggregates, (*b*) disseminated; and (*c*) within veinlets in the exoskarn.

Most of the veins in the Velardeña mining district are not exposed at the surface, they are hosted in the carbonate sequence, generally strike NW–SE and steeply dip to the NE; they have a maximum thickness of 20 m and extend for several km. Some of them suffered brecciation in the proximity of intrusive rocks. They are characterized by an assemblage of calcite and fluorite with subordinate adularia and quartz. The ore minerals contain sphalerite (Fe-poor, pale variety), arsenopyrite and pyrite, with minor galena and chalcopyrite. According to Pinet and Tremblay (2009), these veins are epithermal in origin and are fault controlled. The mineralized structures are cut by NW–SE-striking normal faults related to the Basin and Range extension (Oligocene). The biggest one is a calcite vein-fault located on the boundary between the Antares dike and the Valle de Cuencamé (Figure 2A).

3. Sampling and methods

For this study, 247 rock samples were collected in the Velardeña mining district: 187 from drill cores (139 from Santa María area and 48 from Reyna de Cobre area), 47 in front of the underground mine (28 from Santa María mine and 19 from Reyna del Cobre mine), and 13 in surface outcrops (8 from Santa María area and 5 from Reyna del Cobre area).

Macroscopic description was made of each sample, which allowed a preliminary identification of the essential minerals and a preliminary classification of mineral assemblages and rock types. Ore mineralization was found only in drill cores or underground mine, from which were selected most samples for further analysis (totaling 47 samples; Table 1).

Mineral assemblages were studied in 31 polished thin sections using standard petrographic microscopy. Additionally, all the polished thin sections were analyzed with a Hitachi TM-1000 table-top scanning electron microscope (SEM), at the Natural Resources Department (*Departamento de Recursos Naturales*) of the Geophysical Institute (*Instituto de Geofísica*), National Autonomous University of Mexico (*Universidad Nacional Autónoma de México, UNAM*). This equipment allowed us to obtain back-scattered electron (BSE) images and semi-quantitative chemical analyses by energy dispersive X-ray spectrometry (EDS). Quantitative analyses were obtained with an electron microprobe (EMP) JEOL JXA-8900XR, at the University UNAM (*Laboratorio Universitario de Petrología, UNAM*). Wavelength dispersive spectrometry (WDS) analyses were carried out in the following conditions: (*a*) for silicates: 20 keV, 20 nA, beam diameter of 1 μm, and a counting time of 30 s; the standards we used were biotite (for FeKα, SiKα, MnKα, KKα, TiKα, MgKα) and pyrope (MgKα), chlorite (AlKα) and albite (AlKα), sanidine (BaLα, KKα), plagioclase (CaKα), kaersutite (NaKα, CaKα, SiKα), diopside (CrKα), obsidian (FKα, ClKα), sphalerite (ZnKα) and ilmenite (TiKα, MnKα); (*b*) for carbonates: 15 KeV, 10 nA, beam

SAMPLING AND METHODS

The Velardeña Zn–(Pb–Cu) skarn-epithermal deposits, central-northern Mexico

Table 1. Sample description from the Velardeña district.

n	Sample	Longitude	Latitude	Depth (m)	Orientation	Dip	Location	Classification	Mineral assemblage
1	V-18-E	-103.73514	25.0537146	486	NE 32°	-74.09	Santa María	Calcite vein	Cal, Gn, Sph, Py
2	V-20-D	-103.73452	25.0536352	589	NE 42°	-81.64		Massive mineralization	Py, Sph, Gn, Cpy, Po, Mc, Apy, Hem
3	V-26-B*	-103.74755	25.0573996	321	SW 31°	-45.00		Prograde skarn with Zn-Cu-Pb	Grt, Sph, Py, Cal, Fl, Cpx, Qtz
4	V-36-C	-103.73361	25.0512527	546	NE 33°	-55.14		Quartz vein and breccia	Qtz, Sph, Py, Cpy, Apy, Gn
5	V-39-A*	-103.73296	25.0505071	579	NE 31°	-48.00		Massive mineralization	Sph, Gn, Ccp, Py, Mc, Apy
6	V-48-Q	-103.73297	25.0504791	943	SE 12°	-87.03		Massive mineralization	Sph, Gn, Py, Apy, Cpy, Po
7	V-63-O*	-103.74054	25.0548931	55	NE 34°	-69.60		Breccia	Cal, Grt, Cpx, Qtz, Py
8	V-75-R	-103.73520	25.0550214	399	SW 30°	-84.57		Prograde skarn with Zn-Cu-Pb	Grt, Sph, Cpy, Cal
9	V-78-P*	-103.74146	25.0547911	62	NE 28°	-63.90		Endoskarn	Cpx, Grt, Py, Sd, Cal, Qtz
10	V-81-S	-103.74041	25.057290	419	NE 30°	-59.34		Calcite vein and breccia	Cal, Cpx, Py, Cpy
11	V-86-I	-103.73855	25.0531283	208	NE 31°	-44.89		Altered porphyry	Qtz, Cal, KF, Chl, Apy, Py, Sph
12	V-88-J	-103.73965	25.056486	487	NE 30°	-52.52		Massive mineralization	Py, Sph, Gn, Cpy, Po, Mc, Apy
13	V-90-K	-103.74095	25.0581114	235	NE 30°	-45.00		Altered porphyry	Qtz, Cal, KF, Chl, Apy, Py, Sph
14	V-97-L*	-103.74185	25.0586487	422	NE 29°	-57.03		Altered porphyry	Qtz, KF, Grt, Py, Mc, Cpy
15	V-102-N*	-103.73941	25.0537509	0	-	-		Altered porphyry	Qtz, KF, Chl, Cha
16	V-104-M*	-103.73941	25.0537521	173	NE 29°	-44.30		Quartz vein and breccia	Cal, Qtz, Sph
17	V-122-F	-103.73894	25.0546766	159	NE 30°	-45.60		Calcite vein and breccia	Cal, Cpy, Py, Sph, Grt, Qtz
18	V-129-G*	-103.74287	25.0604005	140	SW 30°	-44.30		Calcite vein	Cal, Sph, Gn, Py
19	V-178-H	-103.72746	25.0484083	335	-	-		Altered porphyry	Qtz, Bt, Cal, Chl, KF, Py, Cpy
20	VE-60-V*	-103.73764	25.0553834	33	NE 31°	-51.22		Calcite vein	Sph, Py, Sd, Qtz
21	VE-02-AD*	-103.73937	25.0540329	78	SW 30°	-29.08		Semi-massive mineralization	KF, Qtz, Po, Sph, Cal, Apy
22	VE-60-Y*	-103.73922	25.0530376	12	NE 29°	-45.59		Calcite vein	Cal, Sph, Py, Po. Cpy, Sd, Qtz
23	VE-122-AC*	-103.73846	25.0531979	38	SW 29°	-18.94		Endoskarn	Sph, Py, Sd, Qtz, Amp
24	VE-122-Z*	-103.73846	25.0532094	4	SW 29°	-56.10		Endoskarn	Sph, Py, Sd, Qtz, Amp, Grt
25	VE-122-AA	-103.73846	25.0532094	13	SW 29°	-56.10		Altered porphyry	Qtz, KF, Py, Mc, Po, Cpy, Apy
26	VE-200-W	-103.73707	25.0539506	4	NE 29°	-36.30		Retrograde skarn	Chl, Ep, Py
27	VE-200-X*	-103.73707	25.0539497	361	NE 29°	-48.50		Altered porphyry	Cal, Qtz, KF
28	VE-200-T	-103.73738	25.053347	66	SW 37°	-55.58		Calcite vein	Cal, Sd, Py, Sph, Gn, Cpy
29	VW-59-U*	-103.73985	25.0542974	56	SW 19°	-30.15		Endoskarn	Cal, Cpx, Grt, Fl, Gn
30	VW-158-AB*	-103.74074	25.0546967	32	SW 29°	-29.53		Calcite and fluorite vein	Fl, Cal, Qtz, Cpx, KF
31	V-05-AF	-103.74996	25.0685188	0	Surface				Qtz, KF, Hem
32	V-06-AG*	-103.72632	25.0404926	0	Surface			Chert	Cal, Qtz
33	UASM-22	undermine		Level 1240	-	-		Massive mineralization	Sph, Gn, Cal
34	C-02-E*	-103.64703	25.0808302	437	SW 44°	-59.18	Reyna de Cobre	Prograde skarn with Zn-Cu-Pb	Ep, Grt, Cal, Sph, Qtz, Fl
35	C-04-F	-103.64535	25.0785862	117	SW 45°	-47.09		Prograde skarn with Zn-Cu-Pb	Qtz, Cal, Sph, KF, Gn
36	C-05-C*	-103.64413	25.0822156	539	SW 44°	-44.70		Prograde skarn with Zn-Cu-Pb	Cal, Qtz, Grt, Po, Py
37	C-05-D	-103.64413	25.0822156	118	SW 44°	-44.70		Endoskarn	Cpx, Grt, Py, Sd, Qtz
38	C-06-A*	-103.64407	25.0822309	474	SW 45°	-57.10		Altered porphyry	Qtz, KF, Cpx, Ep, Chl
39	C-07-B*	-103.65460	25.0829613	267	SW 44°	-42.93		Retrograde skarn	Cal, Grt, Qtz, Chl, Ep
40	C-08-K*	-103.65129	25.0757436	149	NE 44°	-43.37		Retrograde skarn	Wo, Grt
41	C-08-J*	-103.65129	25.0757436	165	NE 44°	-43.37		Altered porphyry	Cal, Grt, Qtz, Cpx
42	C-10-I*	-103.65854	25.0752039	483	NE 35°	-44.47		Endoskarn	Cal, Grt, Cpx, Fl, Sd
43	C-12-H*	-103.64868	25.0831320	586	SE 16°	-52.98		Granitoid (monzogranite)	Qtz, Pl, KF, Bt, Py
44	C-13-G*	-103.64413	25.0773099	250	SW 39°	-44.67		Endoskarn	Cal, Cpx, Wo, KF, Grt
45	C-05-L	undermine		level -5	-	-		Altered porphyry	Pl, Qtz, Bt, KF, Zrn
46	C-07-M	undermine		level -5	-	-		Quartz and calcite vein	Qtz, Cal, Sph
47	C-23-N*	-103.64791	25.0814613	0	Surface			Endoskarn	Grt, Cal, Qtz, Brt

*Mineralogy complemented by X-ray diffraction. Key: Amp — Ca-amphibole; Apy — arsenopyrite; Brt — barite; Cal — calcite; Cha, chabazite; Cpy— chalcopyrite; Chl — chlorite; Cpx — Ca-clinopyroxene; Cpy — chalcopyrite; Ep — epidote; Fl — fluorite; Gn — galena; Grt — Ca-garnet; Hem — hematite; KF — K-feldspar; Mc — marcasite; Po — pyrrhotite; Py — pyrite; Qtz — quartz; Sch — scheelite; Sd — siderite; Sph — sphalerite; Wo — Wollastonite; Zrn — Zircon.

diameter of 1 µm, and a counting time of 30 s; the standards were kaersutite (for KKα, NaKa, MgKa), dolomite (for MnKa, SrLa, FeKa), calcite (for CaKa), sphalerite (for ZnKα) and plagioclase (for BaLα); and (*c*) for sulfides: 20 KeV, 20 nA, beam diameter of 1 µm, and a counting time of 30 s; the standards were skutterudite (NiKα, AsKα, FeKα, CoKα), sphalerite (ZnKα, SnLα), cuprite (CuKα), marcasite (SKα), stibnite (SbLα), Ag (AgLα) and crocoite (PbMα). The number of analyzed points was: adularia, 24; amphibole, 6; calcite, 22; clinopyroxene, 32; fluorite, 14; garnet, 13; galena, 49; pyrite, 63; pyrrhotite, 2; sphalerite, 67.

Bulk mineralogy was determined for 27 samples by X-ray diffraction (XRD), using a Philips 1400 diffractometer located at the Geology Institute (*Instituto de Geología, UNAM*). This instrument is equipped with a Cu anode tube as the X-ray source. The anode tube also directs the collimated Cu Kα1,2 radiation ($\lambda = 0.15405$ nm) towards a randomly oriented sample. X-radiation was generated at 40 kV and 20 mA. Scans were recorded from 4° to 70° (2θ) with a step-scan of 0.02° and 2 s/step. Table 1 summarizes sample locations and mineralogical classifications of the suite of rocks studied in this work.

Fluid inclusions of primary origin (according to the criteria of Roedder 1984) were analyzed in calcite, sphalerite, quartz, garnet and clinopyroxene crystals. Ice melting temperatures (Tm), first, and then homogenization temperatures (T_H) were obtained from fluid inclusions (FI) hosted in calcite, quartz, garnet, clinopyroxene and sphalerite; additionally, halite and clathrate melting temperatures were measured in a few relevant FI. Those FI where leakage, decrepitation, or other modifications were suspected were rejected, following the recommendations of Bodnar *et al.* (1985) and Van-den-Kerkhof and Hein (2001). Salinity values and isochores were calculated assuming an H_2O–NaCl system, using the equations of state of Bodnar and Vityk (1994). Microthermometric studies were carried out on a Linkam THMSG-600 heating-freezing stage at the Geosciences Center (*Centro de Geociencias, UNAM*). Calibration runs show that measurements are accurate to ±0.2 °C for Tm and to ±2 °C for T_H.

Sulfur isotope data were obtained from 21 mineral separates (number of analyses: pyrite, 5; chalcopyrite, 4; sphalerite, 7 and galena, 5). Nearly pure sulfides were separated using a microdrill under a binocular microscope. Samples were analyzed by mass spectrometry using a Delta C Finnigan MAT continuous flow isotope-ratio mass spectrometer interfaced to a TC-EAt elemental analyzer, at the Scientific and Technological Centers of the Barcelona University (*Centres Científics i Tecnològics Universitat de Barcelona, Spain*). The results are given as $\delta^{34}S$‰ values, i.e. per mil deviations relative to the V-CDT (Vienna-Canyon del Diablo Troilite) standard. The analytical precision is within ±0.1‰ at 1 σ.

4. Results

Five broad types of host rocks occur in the Velardeña mining district: altered porphyry, granitoids, marble, limestone and chert. Likewise, mineralization is divided as (*i*) prograde skarn, with disseminated Zn-Cu-Pb mineralization, (*ii*) massive or semi-massive mineralization of Zn-Pb-Cu, (*iii*) retrograde skarn of epidote and chlorite, (*iv*) endoskarn, and (*v*), calcite and quartz veins and breccia (± fluorite and adularia) with Zn-Pb mieralization.

4.1. PARAGENETIC SEQUENCE

Ore-bearing mineral assemblages of Velardeña are rich in calc-silicates and show replacement textures that suggest an epigenetic, sequential mineral deposition (figures 3, 4, and 5) caused by a complex, multistage hydrothermal event. On the basis of the textural microscopic analysis, three paragenetic stages linked to hydrothermal activity can be distinguished (Figure 6): (*a*) prograde skarn, (*b*) retrograde skarn, (*c*) vein filling, and (*d*) supergene stage.
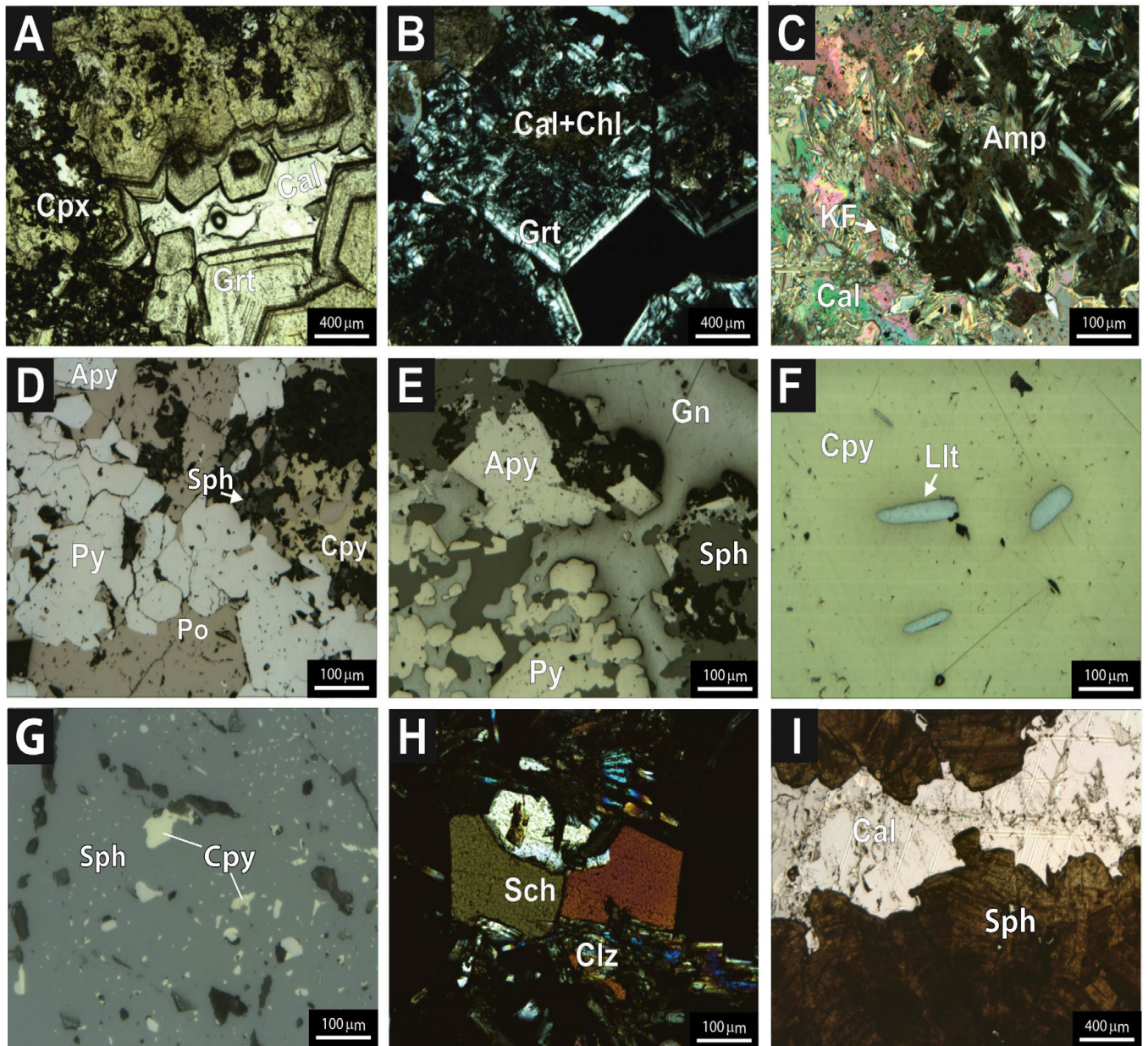
Figure 3 Petrographic images of mineral assemblage representative of the Velardeña ore deposits. (A) Euhedral andradite crystals with concentric zoning, clinopyroxene inclusions, and interstitial calcite (sample C-23-N, transmitted light). (B) Euhedral andradite crystals showing anomalous anisotropy and partial replacement to a calcite-chlorite cryptocrystalline assemblage (sample C-05-C, transmitted light, plane polarized light). (C) Retrograde skarn assemblage with actinolite, adularia, and calcite (sample V-26-B, transmitted light, plane polarized light). (D) Sulfide assemblage of pyrite, arsenopyrite, pyrrhotite, chalcopyrite, and minor Fe-rich sphalerite (Sp-1) (sample V-20-D, reflected light). (E) Sulfide paragenesis of galena, pyrite, sphalerite, and arsenopyrite (sample C-04-F, reflected light). (F) Lillianite prismatic inclusions within chalcopyrite (sample C-05-C, reflected light). (G) Crystals of Fe-poor sphalerite (Sp-2) with chalcopyrite disease (sample VE-60-V, reflected light). (H) Scheelite and clinozoisite from the retrograde skarn assemblages (sample VW-158-AB, transmitted light, plane polarized light). (I) Zoned, subhedral crystals of Fe-poor sphalerite (Sp-2) with calcite, from late vein mineralization (sample V-129-G, transmitted light). Mineral abbreviations: Amp: amphibole (actinolite); Apy: arsenopyrite; Cal: calcite; Chl: chlorite; Clz: clinozoisite; Cpx: clinopyroxene (diopside); Cpy: chalcopyrite; Gn: galena; Grt: garnet (andradite); KF: K-feldspar (adularia); Llt: lillianite; Po: pyrrhotite; Py: pyrite; Sch: scheelite; Sph: sphalerite.

RESULTS
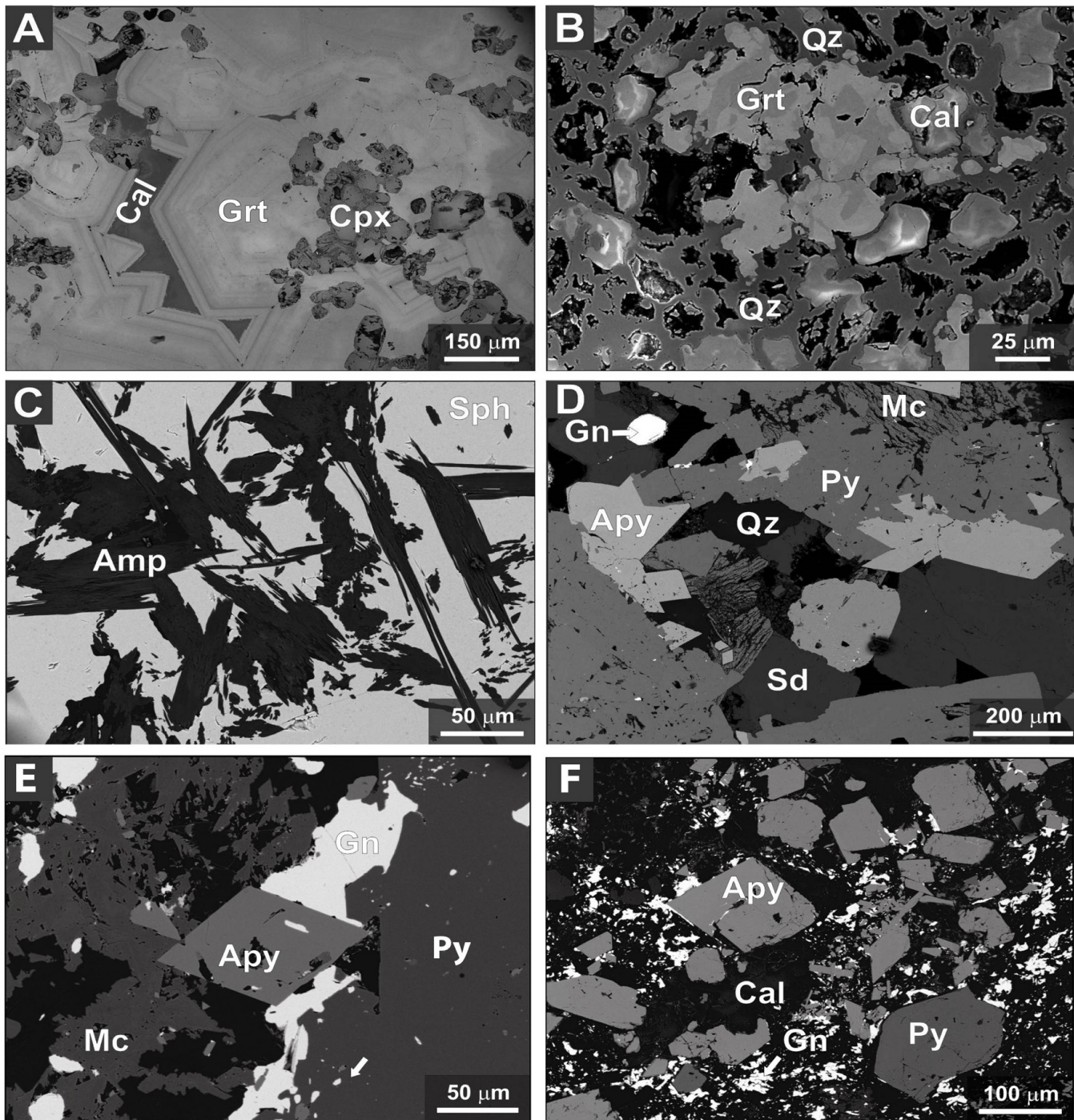
Figure 4 SEM-BSE (secondary electron microscopy in back scattering electrons image) of mineral assemblages of the Velardeña ore deposits. (A) Euhedral andradite crystals with concentric zoning, clinopyroxene inclusions, and interstitial calcite (sample C-23-N). (B) Relic andradite replaced by a quartz-calcite assemblage (sample V-122-F). (C) Actinolite acicular crystals within a sphalerite groundmass (sample V-26-B). (D) Pyrite–arsenopyrite paragenesis followed by a late (supergene), replacive siderite–marcasite assemblage (sample V-88-J). (E) Sulfide paragenesis of galena, pyrite, arsenopyrite, and marcasite, (sample C-04-F). (F) Assemblage of pyrite, arsenopyrite, and galena crystals; galena is located in fractures and grains boundaries (sample C-04-F). Mineral abbreviations: Amp: amphibole (actinolite); Apy: arsenopyrite; Cal: calcite; Cpx: clinopyroxene (diopside); Gn: galena; Grt: garnet (andradite); Mc: marcasite; Py: pyrite; Qz: quartz; Sd: siderite; Sph: sphalerite.

The Velardeña Zn–(Pb–Cu) skarn-epithermal deposits, central-northern Mexico

During the prograde stage calcic clinopyroxene and garnet formed in the exoskarn; clinopyroxene usually occurs as inclusions in poikilitic garnet crystals, both in Reyna de Cobre and in Santa María (figures 3a, 3b, and 4a), which implies that garnet formed relatively later than clinopyroxene (Figure 4a). Garnet crystals are euhedral with concentric zoning and anomalous anisotropy, and rarely exceed 3 mm in diameter, whereas clinopyroxenes occur as short prismatic crystals, up to 300 μm in length. Wollastonite, which is particularly abundant in the endoskarn, occurs as veinlet infills and pseudomorphs after plagioclase, and also occurs with quartz and calcite.

During the retrograde stage hydrous silicates (calcic amphibole, epidote and chlorite), sulfides (pyrite, arsenopyrite, sphalerite, galena, chalcopyrite, and pyrrhotite) and sulfosalts (lillianite, $Pb_3Bi_2S_6$; and boulangerite, $Pb_5Sb_4S_{11}$), as well as scheelite, hematite, quartz and calcite were deposited (figures 3c to 3h). Such assemblages occur interstitially with respect to clinopyroxene and garnet and may pseudomorphically replace the latter (Figure 4b).

Calcic amphibole occurs mostly as acicular crystals, up to 1 mm in length, which are generally included in sphalerite and galena grains (Figure 4c), as single crystals, or forming radial aggregates. Epidote forms prisms up to 700 μm long (Figure 3h) and commonly replaces calcic garnets in the exoskarn and plagioclase phenocrysts in the endoskarn. Chlorite is found as radial aggregates, up to ~50 μm in diameter, replacing calcic garnets and filling veinlets (Figure 3b). Sphalerite and galena are the most abundant sulfides. Sphalerite occurs through all the mineralized zones. In veins, sphalerite develops anhedral crystals, up to a few centimeters across, with curvilinear equilibrium grain boundaries. In the massive or semimasive mineralization it forms mosaic aggregates and intergrowths with galena, pyrrhotite, pyrite and chalcopyrite, which can be interpreted as a coge-
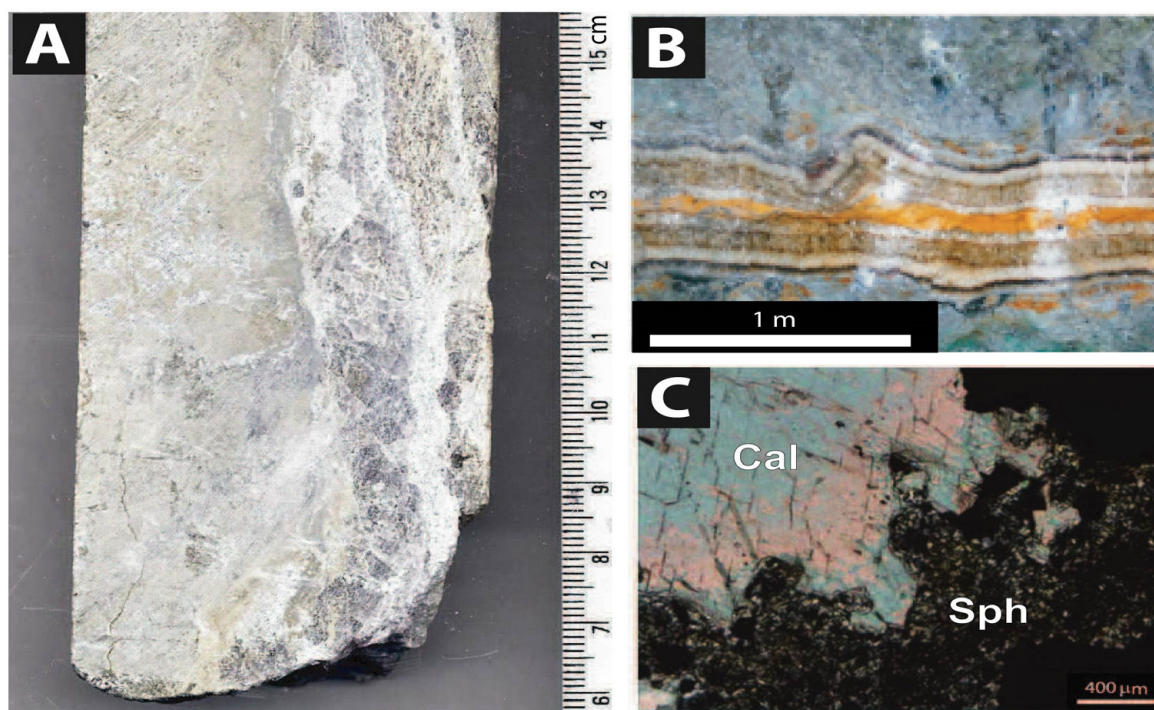
Figure 5 (A) Core sample showing epithermal vein of calcite (white) and fluorite (purple gray) cutting the skarn assemblage from the Santa Maria deposit (sample VW-158 AB). (B) Epithermal vein inside the Santa Maria mine, where several generations of growth are exhibited. (C) Photomicrograph of the sphalerite crystals in calcite vein (sample V-129-G, transmitted light, plane polarized light). Cal: calcite; Sph: sphalerite.

netic association (Gilmer *et al.*, 1988). Galena is generally associated with sphalerite and commonly has boulangerite intergrowths. Galena occurs in all the mineralized zones. At the microscopic level, galena veinlets crosscut pyrite, sphalerite, chalcopyrite and pyrrhotite.

Pyrite and pyrrhotite are widespread in the massive ores, occurring in a large variety of textures and grain sizes. The grain size of pyrite is up to 0.5 mm, while pyrrhotite is up to 200 μm. In the exoskarn, pyrite occurs as coarse-grained aggregates of euhedral crystals with interstitial calcite, chlorite and quartz in cogenetic association with sphalerite and minor galena (Figures 3d and 3e). In the endoskarn pyrite occurs as pseudomorphs after plagioclase phenocrysts (Figure 4d).

The final hydrothermal stage produced the vein and breccia mineralization that crosscut the previous skarn paragenesis (Figure 5b). This late mineralization is also complex, being the product of a succession of events, which resulted in multiple vein generations and in a variety of structures

as brecciation, open-filling texture and crustiform banding. Veins are mostly filled by calcite and quartz, with fluorite and adularia also abundant (Figure 5a). Quartz occurs both as microcrystalline anhedral aggregates and as chalcedony, whereas calcite commonly forms mosaic aggregates. Adularia develops rhomb-shaped crystals, up to 1 mm across, and occurs disseminated within the calcite aggregates, associated with quartz. Veins hosted in porphyritic rocks show alteration halos with sericite, chlorite and chabazite (Figure 3c).

Some of the veins are rich in fluorite, which occurs as monomineralic bands alternating with quartz. A pale, Fe-poor variety of sphalerite is also characteristic of vein mineralization and forms two different open-filling textures (Figure 5c): (*a*) subhedral crystals, up to 1 cm across with concentric zoning (Figure 3i), and (*b*) botryoidal aggregates. Other ore minerals that are present in veins and breccias are arsenopyrite, pyrite and marcasite, in addition to subordinate galena and chalcopyrite.
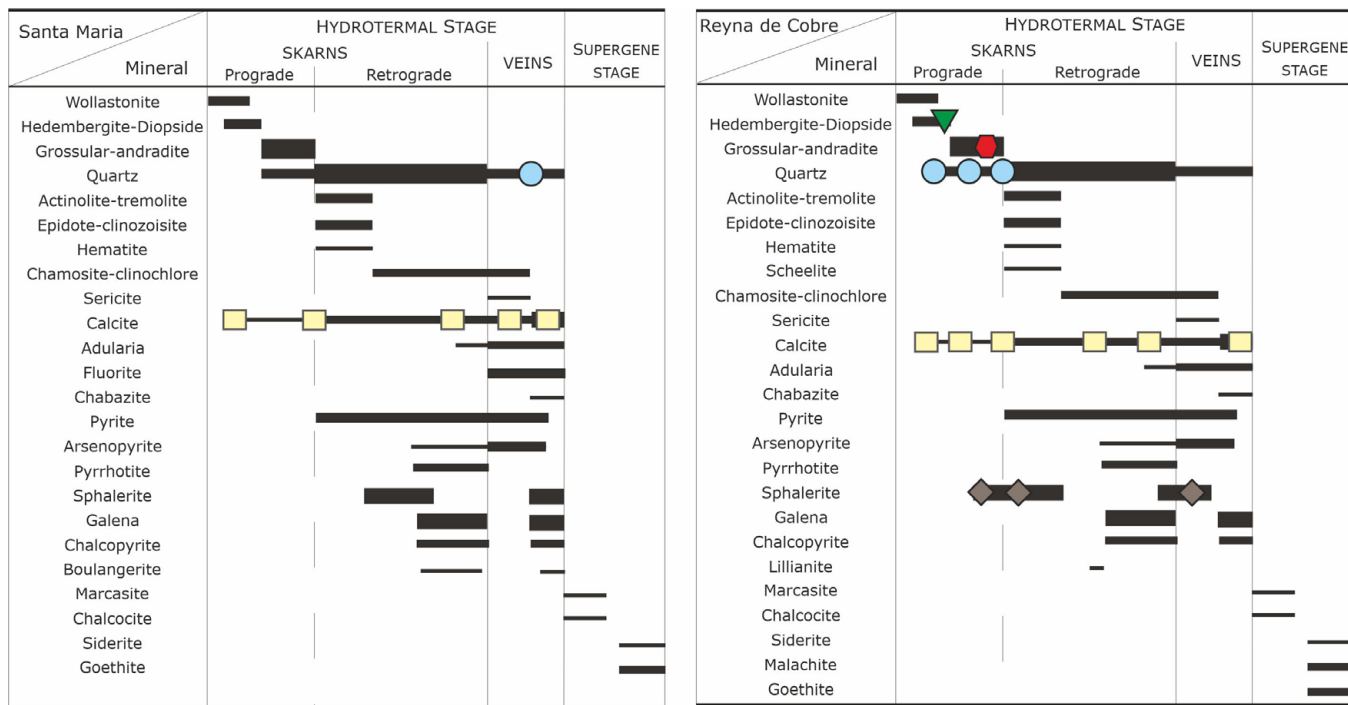

Figure 6 Comparative paragenetic tables of the Velardeña skarn and vein deposits. Left: Santa Maria deposit. Right: Reyna del Cobre deposit. Symbols: quartz: circles; calcite: squares; amphibole: triangles; garnet: hexagon; sphalerite: diamond. All colored symbols are related to temperatures in Figures 10 and 12. Black bars thickness corresponds to relative abundance of minerals.

4.2. MINERAL CHEMISTRY

4.2.1. CALCIC AMPHIBOLE

The Fe content in the amphiboles ranges from 0.844 to 0.745 atoms per formula unit (apfu), while Mg varies between 4.048 and 4.072 apfu (Table 2). According to the classification of Leake *et al.* (2004), all the analyzed crystals correspond to actinolite (Figure 7a).

Additionally, according to the latest nomenclature of the amphibole group of Hawthorne *et al.* (2012), the crystals plot between the cummingtonite and actinolite fields, because they are depleted in manganese (0.04 to 0.055 apfu; Table 2 and Figure 7b).

4.2.2. CALCIC CLINOPYROXENE

The clinopyroxene crystals have Fe contents between 0.019 and 0.431 apfu, Mg from 0.544 to 0.978 apfu, and Mn up to 0.045 apfu (Table 3; Figure 7c). They belong to the diopside–hedenbergite series ($Di_{97-53}Hd_{42-02}Jh_{04-01}$; Figure 7d) and are classified as diopside (cf. Morimoto *et al.*, 1988).

4.2.3. CALCIC GARNET

Although all the analyzed garnets are andradite, their composition is variable ($Ad_{100-57}Grs_{43-00}$), as reflected in their concentric zoning, the "pyralspite" component ($Mg+Mn+Fe^{2+}$) being very low, up to 2.3 mol %. All crystals plotted in the field of Zn skarns (Meinert *et al.,* 2005) (Figure 7e; Table 3).

4.2.4. K-FELDSPAR

The crystals of K-feldspar correspond to the adularia variety (*i.e.,* crystals with some degree of order between orthoclase and microcline, usually crystallized from hydrothermal fluids; Dal-Negro
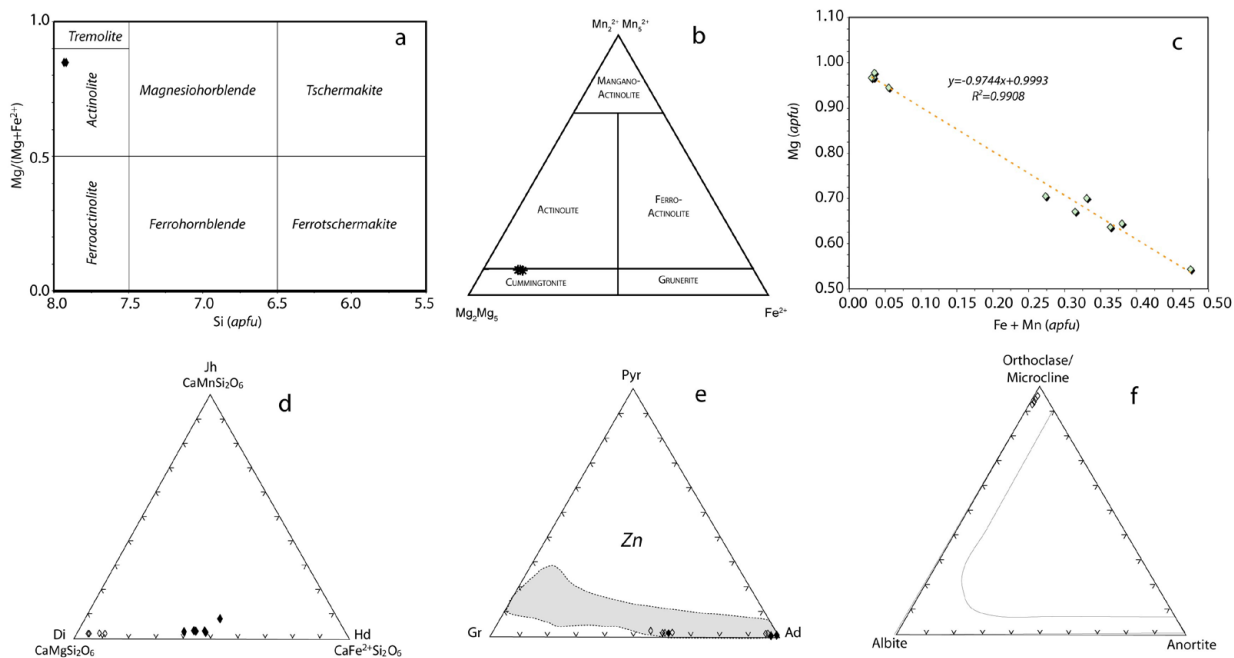
Figure 7 Composition diagrams of silicates (electron-microprobe data) from the Velardeña skarns. (a) Amphibole plot of Leake et al. (2004). (b) Magnesium-iron-manganese amphiboles classification of calcium amphiboles of Hawthorne et al. (2012). (c) Mg vs. Fe + Mn correlation in calcic clinopyroxenes. (d) Calcic clinopyroxenes plotted on johannsenite (Jh)–diopside (Di)–hedenbergite (Hd) triangular diagram. (e) Calcic garnets plotted on a pyralspite (Pyr)–grossular (Gr)–andradite (Ad) triangular diagram; dashed area indicates the composition range for Zn skarn deposits worldwide compiled by Meinert et al. (2005). (f) K-feldspar (adularia) plotted on orthoclase–albite–anorthite triangular diagram. Black diamonds correspond to Reyna de Cobre samples, while empty diamonds correspond to Santa María samples; apfu: atoms per formula unit.

et al., 1978). Compositionally, they are classified as $Or_{96-92}Ab_{08-04}An_{00}$ (Figure 7f), with barium not exceeding ~0.50 wt.% (Table 3).

4.2.4. SULFIDES

The ore assemblage of Velardeña essentially consists of sphalerite, galena, chalcopyrite, pyrite, arsenopyrite, pyrrhotite, and Bi- and Sb-sulfosalts (figures 3, 4d, and 4e).

Pyrrhotite EMP analyses yield a chemical composition close to Fe_7S_9 (ca. 44.4 atom % of Fe; 55.6 atom % of S). Such composition corresponds to the monoclinic polytype of pyrrhotite (cf. Lusk *et al.*, 1993).

Arsenopyrite forms up to 0.5 mm long euhedral crystals. Chemically, the crystals approximate the ideal formula of pure arsenopyrite, FeA_sS, with 32.6 to 33.4 atom % of As.

The galena composition matches that of pure galena, PbS, although the analyses revealed a silver contents ranging between 0.40 and 0.21 wt.% (figures 3e, 4e, and 4f).

Two modes of occurrence of sphalerite, corresponding to different stages of the mineralization, can be recognized (Figure 8): (*a*) *Sp-1*, associated with calc-silicates, corresponding to the marmatite (dark) variety; and (*b*) *Sp-2*, in calcite–fluorite veins and breccias, corresponding to the pale variety. In both cases, sphalerite is intergrown with galena, and *Sp-2* has "chalcopyrite disease" texture. Chemically, there are significant differences between *Sp-1* and *Sp-2*, particularly in the iron contents (Figure 8b; Table 4). Iron shows a wide range of variation in the crystals (from 2.69 to 12.61 wt.% Fe), so that the highest concentrations (16–22 mol % FeS) correspond to sphalerite that is associated with garnet skarns (*Sp-1*), whereas sphalerite from veins (*Sp-2*) is iron-poor (4–6 mol % FeS), which is in agreement with the two varieties that were optically identified. In contrast, other elements such as cadmium (<0.223 atom % of Cd) and manganese (0.136–2.219 atom % of Mn) are in low concentrations and do not show significant variations between the two sphalerite types.

Table 2. Chemical composition and structural formulas of calcic amphiboles from the Velardeña skarn deposits (sample V-26-B, Table 1).

		#1	#2	#3
SiO_2	wt.%	57.48	58.72	57.96
Al_2O_3		0.71	0.80	0.95
TiO_2		0.03	0.02	0.00
CaO		13.90	13.02	13.03
Na_2O		0.15	0.17	0.17
K_2O		0.14	0.12	0.17
MnO		0.47	0.45	0.38
FeO		6.81	6.54	7.37
MgO		19.70	20.05	19.82
NiO		0.00	0.00	0.01
Cr_2O_3		0.00	0.00	0.00
H_2O*		2.17	2.20	2.19
Total		101.54	102.08	102.04
Si	apfu	7.92	8.00	7.94
Al		0.12	0.13	0.15
Ti		0.00	0.00	0.00
Ca		2.05	1.90	1.91
Na		0.04	0.04	0.04
K		0.02	0.02	0.03
Mn^{2+}		0.05	0.05	0.04
Fe^{2+}		0.79	0.75	0.84
Mg		4.05	4.07	4.05
Ni		0.00	0.00	0.00
Cr		0.00	0.00	0.00

Apfu: atoms per formula unit. H_2O based on structural formula 22 O, 2 OH.

The sphalerite geobarometer of Hutchinson and Scott (1981) has been applied to three analyses (#10, 11, and 12 of Table 4) that were selected because they correspond to *Sp-1* crystals and where found in paragenesis with pyrite and pyrrhotite (figures 3d and 3e). The pressure thus obtained is 0.8–0.9 kbar, corresponding to a depth of ~3–4 km.

4.2.6. CARBONATES

Carbonate minerals occur in veins and in interstitial position with respect to silicates and sulfides

RESULTS

The Velardeña Zn–(Pb–Cu) skarn-epithermal deposits, central-northern Mexico

Table 3. Chemical composition and structural formulas of selected silicates from the Velardeña skarn deposits (#1 from sample C-04-F; #2 to #3 from VW-158-AB, #4 to #7 from C-23-N; #9 from C-02-E; #10 to #12 from V-26-B, Table 1).

		Kfs #1	Kfs #2	Px #3	Px #4	Px #5	Px #6	Px #7	Grt #8	Grt #9	Grt #10	Grt #11	Grt #12
SiO_2	wt. %	65.24	65.99	53.16	54.97	54.92	54.83	55.28	32.52	34.35	35.31	34.97	34.78
Al_2O_3		17.03	17.55	0.85	0.31	0.41	0.26	0.29	0.25	8.69	0.05	0.00	0.41
TiO_2		0.00	0.00	0.01	0.00	0.00	0.01	0.00	0.00	1.58	0.01	0.00	0.05
CaO		0.00	0.00	24.56	25.97	26.06	25.89	26.08	33.23	34.37	32.96	33.07	33.05
Na_2O		0.51	0.78	0.22	0.00	0.00	0.00	0.00	n.a.	n.a.	n.a.	n.a.	n.a.
K_2O		16.17	15.61	0.00	0.00	0.00	0.00	0.00	n.a.	n.a.	n.a.	n.a.	n.a.
BaO		0.24	0.46	n.a.	n.a.	n.a.	n.a.	n.a.	n.a.	n.a.	n.a.	n.a.	n.a.
MnO		0.04	0.00	0.52	0.20	0.30	0.31	0.39	0.17	0.43	0.13	0.14	0.14
Fe_2O_3		n.a.	n.a.	n.a.	n.a.	n.a.	n.a.	n.a.	31.77	17.91	32.35	32.36	31.51
FeO		0.57	0.01	9.54	1.62	0.82	0.85	0.63	n.a.	n.a.	n.a.	n.a.	n.a.
MgO		0.00	0.00	12.06	17.54	17.99	18.14	18.03	0.16	0.33	0.00	0.00	0.03
NiO		n.a.	n.a.	0.00	0.00	0.02	0.03	0.01	0.01	0.16	0.00	0.00	0.01
Cr_2O_3		n.a.	n.a.	0.00	0.00	0.00	0.01	0.00	0.00	0.14	0.00	0.00	0.00
Total		99.80	100.40	100.92	100.61	100.51	100.32	100.71	98.10	97.96	100.82	100.54	99.98
Si	apfu	3.03	3.04	1.98	1.99	1.98	1.98	1.99	2.81	2.81	2.97	2.95	2.94
Al		0.93	0.95	0.04	0.01	0.02	0.01	0.01	0.02	0.02	0.01	0.00	0.04
Ti		0.00	0.00	0.00	0.00	0.00	0.00	0.00	0.00	0.00	0.00	0.00	0.00
Ca		0.00	0.00	0.98	1.01	1.01	1.00	1.01	3.07	3.07	2.97	2.99	2.99
Na		0.05	0.07	0.02	0.00	0.00	0.00	0.00	-	-	-	-	-
K		0.96	0.92	0.00	0.00	0.00	0.00	0.00	-	-	-	-	-
Ba		0.00	0.01	-	-	-	-	-	-	-	-	-	-
Mn^{2+}		0.00	0.00	0.02	0.01	0.01	0.01	0.01	0.01	0.01	0.01	0.01	0.01
Fe^{2+}		0.02	0.00	0.30	0.05	0.02	0.03	0.02	-	-	-	-	-
Fe^{3+}		-	-	-	-	-	-	-	2.06	2.06	2.05	2.05	2.01
Mg		0.00	0.00	0.67	0.95	0.97	0.98	0.97	0.02	0.02	0.00	0.00	0.00
Ni		-	-	0.00	0.00	0.00	0.00	0.00	0.00	0.00	0.00	0.00	0.00
Cr		-	-	0.00	0.00	0.00	0.00	0.00	0.00	0.00	0.00	0.00	0.00

Apfu: atoms per formula unit. Grt: Ca garnets (structural formula based on 12 O); andradite. Px: Ca clinopyroxenes (structural formula based on 6 O); diopside. Kfs: K feldspars (structural formula based on 8 O); adularia. n.a.: not analyzed.

RESULTS

Table 4. Chemical composition and structural formulas of selected sphalerite from the Velardeña skarn and vein deposits (#1 to #2 from sample V-39-A; #3 to #6 from V-18-E; #7 to #9 from V-129-G; 10 to 12 from VE-02-AD, Table 1).

		Sp-1 #1	Sp-1 #2	Sp-1 #3	Sp-1 #4	Sp-1 #5	Sp-1 #6	Sp-2 #7	Sp-2 #8	Sp-2 #9	Sp-1 #10	Sp-1 #11	Sp-1 #12
S	*wt. %*	33.89	33.58	33.79	33.78	33.62	33.61	33.05	33.60	33.62	33.92	33.47	33.78
Mn		0.75	0.72	0.24	0.21	0.21	0.18	2.46	0.49	0.56	0.44	0.39	0.38
Cu		0.00	0.02	0.02	0.07	0.07	0.02	0.00	0.06	0.05	0.01	0.00	0.02
As		0.019	0.002	0.05	0.00	0.03	0.02	0.00	0.00	0.00	0.00	0.00	0.01
Bi		0.02	0.00	0.00	0.00	0.02	0.03	0.00	0.00	0.07	0.00	0.14	0.00
Fe		12.08	12.06	11.43	11.65	11.68	11.59	2.77	3.16	3.08	11.40	11.30	11.41
Cd		0.08	0.04	0.06	0.09	0.03	0.00	0.52	0.23	0.33	0.14	0.06	0.01
Zn		53.081	53.242	54.2	53.9	53.9	54.4	61.16	62.6	62.47	54.239	54.31	54.2
Sn		0.00	0.00	0.00	0.00	0.00	0.02	0.06	0.04	0.09	0.00	0.00	0.00
Ag		0.00	0.00	0.00	0.00	0.00	0.00	0.00	0.00	0.00	0.00	0.00	0.00
Sb		0.01	0.00	0.00	0.00	0.00	0.00	0.00	0.00	0.00	0.02	0.03	0.01
Pb		0.00	0.00	0.00	0.05	0.09	0.06	0.017	0.00	0.00	0.00	0.00	0.00
Total		99.93	99.66	99.81	99.75	99.65	99.92	100.03	100.16	100.26	100.17	99.69	99.82
S	*atom %*	50.34	50.09	50.34	50.36	50.2	50.11	49.90	50.53	50.57	50.36	50.06	50.31
Mn		0.65	0.63	0.21	0.19	0.18	0.15	2.17	0.43	0.49	0.38	0.34	0.33
Cu		0.00	0.02	0.01	0.05	0.05	0.01	0.00	0.04	0.04	0.00	0.00	0.01
As		0.01	0.00	0.03	0.00	0.02	0.01	0.00	0.00	0.00	0.00	0.00	0.01
Bi		0.00	0.00	0.00	0.00	0.01	0.01	0.00	0.00	0.02	0.00	0.03	0.00
Fe		10.30	10.32	9.78	9.97	10	9.92	2.40	2.73	2.66	9.71	9.71	9.76
Cd		0.03	0.01	0.03	0.04	0.01	0.00	0.22	0.10	0.14	0.06	0.02	0.00
Zn		38.65	38.93	39.60	39.39	39.5	39.75	45.28	46.16	46.06	39.47	39.82	39.57
Sn		0.00	0.00	0.00	0.00	0.00	0.01	0.02	0.02	0.04	0.00	0.00	0.00
Ag		0.00	0.00	0.00	0.00	0.00	0.00	0.00	0.00	0.00	0.00	0.00	0.00
Sb		0.00	0.00	0.00	0.00	0.00	0.00	0.00	0.00	0.00	0.01	0.01	0.00
Pb		0.00	0.00	0.00	0.01	0.02	0.01	0.00	0.00	0.00	0.00	0.00	0.00

The Velardeña Zn–(Pb–Cu) skarn-epithermal deposits, central-northern Mexico

Table 5. Summary of fluid inclusions microthermometric data from the Velardeña skarn deposits.

Sample	Location	Stage	Mineral	#	FIA	Th (°C) min./mean/max.	Tm (°C) max./mean/min.	Salinity (wt.% NaCl eq.) min./mean/max.
VW-158-AB	Santa María	vein	Cal	18	a	144/156/179	8.1/7.2/6.1*	4/5/7
V-36-C		vein	Qtz	9	-	130/134/138	-14.0/-14.0/-14.0	18/18/18
V-81-S		vein	Cal	17	b	120/148/184	-18.0/-19.5/-21.0	21/22/23
V-81-S		retrograde	Cal	16	d	400/413/458	-18.0/-20.0/-23.0**	30/32/33
VE-200-T		prograde	Cal	11	c	365/413/468	-11.0/-13.5/-16.0	15/17/19
V-129-G		prograde	Cal	18	c	289/343/420	-13.0/-14.4/-19.8	17/18/21
V-02-AD		prograde	Cal	13	c	230/250/268	-7.0/-12.4/-15.5	11/16/19
+RC-N9 # 5	Reyna de Cobre	prograde	Qtz	28	b	395/376/400	-14.5/-14.5/-14.5	18/18/18
+RC-N9 # 5		prograde	Cal	15	c	260/370/480	-22.0/-27.5/-35.0**	32/35/40
+RC-N7#4		prograde	Cal	3	b	295/297/300	-8.7/-8.7/-8.7	13/13/13
+RC-N5#5		prograde	Cal	8	b	290/340/390	-8.0/-9.9/-13.3	12/14/17
+RC-N5#5		prograde	Cal	16	a	295/299/306	-23.2/-24.8/-29.2**	33/34/36
+RC #1		prograde	Cal	18	c	234/315/353	-21.0/-23.4/-26.0**	31/34/35
+RC #2		prograde	Qtz	23	c	294/386/396	-6.9/-6.9/-6.9	10/10/10
+RC #2		prograde	Cpx	9	b	375/455/475	-14.7/-14.7/-14.7	18/18/18
+RC #3		prograde	Cal	20	b	284/370/388	-1.0 /-6.7-7.0	13/13/13
C-02-E		vein	Sp-2	10	-	170/186/196	-17.0/-18.9/-20.0	20/21/22
C-02-E		prograde	Cal	32	a	288/324/346	-16.8/-17.6/-21.0	20/21/23
C-02-E		prograde	Grt	11	b	337/352/376	-13.0/-14.9/-18.0	17/19/21
C-04-F		retrograde	Cal	11	b	240/249/256	-13.0/-13.7/-14.9	17/18/19
C-04-F		prograde	Sp-1	8	b	310/345/390	-12.0/-13.1/-14.0	16/17/18
C-07-M		retrograde	Cal	21	b	236/260/286	-10.8/-12.5/-14.0	15/16/18
C-07-M		prograde	Qtz	12	a	296/318/334	-17.7/-19.9/-21.0	21/22/23
+RC-N5#1		retrograde	Cal	20	b	232/269/297	-4.5/-5.2/-9.5	7/8/13
+RC-N5#2		retrograde	Cal	4	b	220/229/244	-4.2/-10.2/-14.7	7/14/18
+RC-N8#6		retrograde	Cal	15	b	259/269/295	-12.0/-12.0/-12.0	16/16/16
+RC #7		vein	Cal	7	a	100/120/148	5.0/3.3/1.3*	9/11/14

Key: Th =temperature of homogenization, Tm =temperature of ice melting (freezing point depression), * clathrate melting, **halite melting. # =number of analyzed inclusions, min. =minimum value, max. =maximum value. Abbreviations: Cal — calcite; Cpx — Ca clinopyroxenes; Grt — Ca garnets; Qtz — quartz; Sp — Sphalerite.
+samples for FI study in Reyna de Cobre (undermine) from levels 1, 2, 3, 5, 7, 8 amd 9.

(figures 3a, 3g, and 3i). Chemically, these carbonates vary between near pure calcite to manganoan calcite, with up to 3.3 mol % MnCO3.

4.3. FLUID INCLUSIONS

The FI have regular morphologies and are distributed following growth zones of crystals, or isolated, ranging in size from 5 to 25 μm. In the skarn assemblages, the FI are aqueous with two phases (liquid + vapor) (Figure 9a). In late vein calcite, some FI are poly-phased (liquid + vapor + solid), the solid being always halite (figures 9b, 9c, and 9d). CO_2 was detected in some FI, particularly in the veins, through the formation of clathrates, which implies that this gas is above 3.7 wt.% (cf. Hedenquist and Henley, 1985).

The microthermometric data are summarized in Table 5 and plot on a T_H versus salinity diagram shown in Figure 10.

4.3.1. REYNA DE COBRE FLUID INCLUSIONS

In the Reyna de Cobre samples, it was possible to measure FI hosted by clinopyroxene crystals, which yield the highest T_H, from 375 to 475 °C, and salinity values of 18 wt.% NaCl eq. It was also possible to obtain results from garnet crystals, with T_H from 337 to 376 °C and salinity from 17 to 21 wt.% NaCl eq. (Figure 10a; Table 5).

Microthermometry data from quartz distribute in the T_H–salinity space in three clusters that correspond to three different FI assemblages (FIA): (*a*) T_H between 296 and ~335 °C and salinity of 21–23 wt.% NaCl eq., (*b*) T_H of 395–400 °C and salinity ~18 wt.% NaCl eq., and (*c*) T_H of 294–396 °C and salinity ~10 wt.% NaCl eq. The widest range of variation of T_H and salinity is displayed by calcite-hosted FI, which define three clusters of data that partly overlap those above: (*a*) low T_H and intermediate salinity, with 100–148 °C, and 9–14 wt.% NaCl eq.; (*b*) medium to high T_H and low to high salinity, with 220–390 °C, and 2–23 wt.% NaCl eq.; and (*c*) high T_H and very high salinity, with 234–353°C, and 32–38 wt.% NaCl eq. (Figure 10; Table 5).
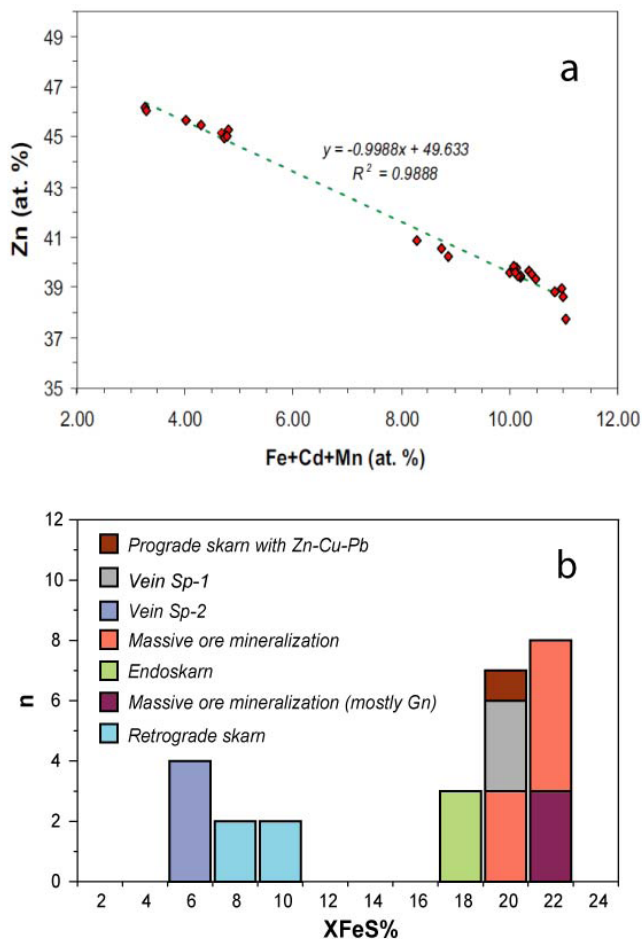
Composition diagrams of all sphalerite crystals (n = 67, electron microprobe data) from the Velardeña skarns and veins. (a) Zn vs. Fe + Cd + Mn plot, where 2 sphalerite types are plotted. (b) Histogram of iron contents, in X% FeS.

Two different populations of sphalerite FI are revealed in the T_H versus salinity plot, having a correspondence with the two sphalerite types (figures 3g and 10a; Table 5): (*a*) *Sp-1*: T_H of 310–390 °C and salinity of 16–18 wt.% NaCl eq., and (*b*) *Sp-2*: T_H of 170–196 °C and salinity of 20–22 wt.% NaCl eq.

4.3.2. SANTA MARIA FLUID INCLUSIONS

In the Santa María mineralized area, we found analyzable quartz-hosted FI exclusively in vein samples, with a range of T_H of 130–138 °C and salinity of 18 wt.% NaCl eq. As for calcite, four clusters of data are defined in a T_H–salinity binary plot (Figure 10b, Table 5): (*a*) low T_H and low salinity, with 144–179 °C, and 4–7 wt.% NaCl

Table 6. Sulfur isotope data, δ³⁴S (‰), for sulfide minerals from the Velardeña skarn deposits.

Sample	Location	Stage	Classification	$\delta^{34}S_{(CTD)}$			
				Cpy	Gn	Sph	Py
C-O2-D	Reyna de Cobre	prograde	*Prograde skarn with Zn-Cu-Pb*		0.9		2.2
C-O4-F		vein	*Prograde skarn with Zn-Cu-Pb*			1.3	
C-O4-F		prograde	*Prograde skarn with Zn-Cu-Pb*				2.6
C-O4-F		vein	*Prograde skarn with Zn-Cu-Pb*	-0.0			
V-18-E	Santa María	retrograde	*Calcite vein*			0.7	
V-20-D		prograde	*Massive mineralization*	0.8			
V-20-D		prograde	*Massive mineralization*		-0.9		
V-26-B		prograde	*Prograde skarn with Zn-Cu-Pb*			-1.1	
V-39-A		prograde	*Massive mineralization*		0.9		
V-39-A		prograde	*Massive mineralization*	1.0			
V-39-A		prograde	*Massive mineralization*		-0.5		
VE-60-V		vein	*Calcite vein*			-0.9	
V-75-R		prograde	*Prograde skarn with Zn-Cu-Pb*			0.6	
V-75-R		prograde	*Prograde skarn with Zn-Cu-Pb*	-0.7			
V-78-P		prograde	*Endoskarn*				-0.5
V-88-J		retrograde	*Massive mineralization*				1.0
V-122-AC		prograde	*Endoskarn*	0.9			
V-129-G		vein	*Calcite vein*			1.8	
VE-200T		vein	*Calcite vein*				0.7
UASM-22		retrograde	*Massive mineralization*			-3.9	

Key: Cpy, chalcopyrite; Gn, galena; Py, pyrite; Sph, sphalerite.

eq.; (*b*) low T_H and high salinity, with 120–184 °C, and 22–23 wt.% NaCl eq.; (*c*) medium to high T_H and high salinity, with 230–468 °C, and 10–21 wt.% NaCl eq.; and (*d*) high T_H and very high salinity, with 400–458 °C, and 30–33 wt.% NaCl eq., (equivalent to FIA (c) of the Reyna de Cobre deposit).

4.3.3. SULFUR ISOTOPES

Sulfur isotopic composition of sulfides is presented in Figure 11 and Table 6. All δ³⁴S values are distributed in a short range, between -1.1 and +2.6‰, except one value of -3.9‰ that corresponds to sphalerite of the late generation (*Sp-2*), from a vein of the Santa María mineralized area (sample VASM-22 of Table 6).

In one sample from Reyna de Cobre (C-04-F of Table 6), pyrite and galena occur apparently in paragenesis (figures 3e, 4e, and 4f) and have been isotopically analyzed, with δ³⁴S of +2.6 and 0.0‰, respectively. The temperature of formation of this mineral pair was calculated with the isotopic geo-themometer of Ohmoto and Rye (1979), with a result of 346 ±25 °C.

5. Discussion

5.1. TYPE OF DEPOSIT

The two studied skarn occurrences of Velardeña (Santa María and Reyna de Cobre) are very similar in terms of structure and mineral composition. In

both areas, skarns occur along the intrusive contact between stocks (and dikes) and limestones and are largely composed by andradite garnet accompanied by Zn–Pb (Cu) sulfides. These characteristics allow us to categorize them as zinc skarns (Einaudi *et al.*, 1981; Meinert *et al.*, 2005). Considering (*a*) the nature of the precursor magmatism (dikes and stocks of porphyritic texture; granitic to granodioritic composition), and (*b*) that skarns develop as aureoles around the intrusive contact, the studied mineralization can also be characterized as proximal, dike-related skarn deposits (Einaudi *et al.*, 1981).

The calculated pressure for the Velardeña skarns using the sphalerite geothermometer of Hutchinson and Scott (1981), 0.8–0.9 kbar, confirms that they formed at hypabyssal depths in the crust (i.e., less than 5 km). Moreover, shallow skarns (<1 kbar) are typically Zn- and Pb-rich, this being the case of Velardeña, whereas deeper skarns (1–3 kbar) are generally Cu-rich (Shimazaki, 1975).

On the other hand, the chemical composition of garnets plotted in a ternary diagram ("pyralspite"–andradite–grossular) fall, for both studied occurrences, in the field of Zn skarn deposits summarized by Meinert *et al.* (2005) (Figure 7e).

5.2. PROCESSES AND CONDITIONS OF FORMATION

Skarn deposits form by metasomatism, through a succession of replacive mineralizing events triggered by a magmatic-hydrothermal system,
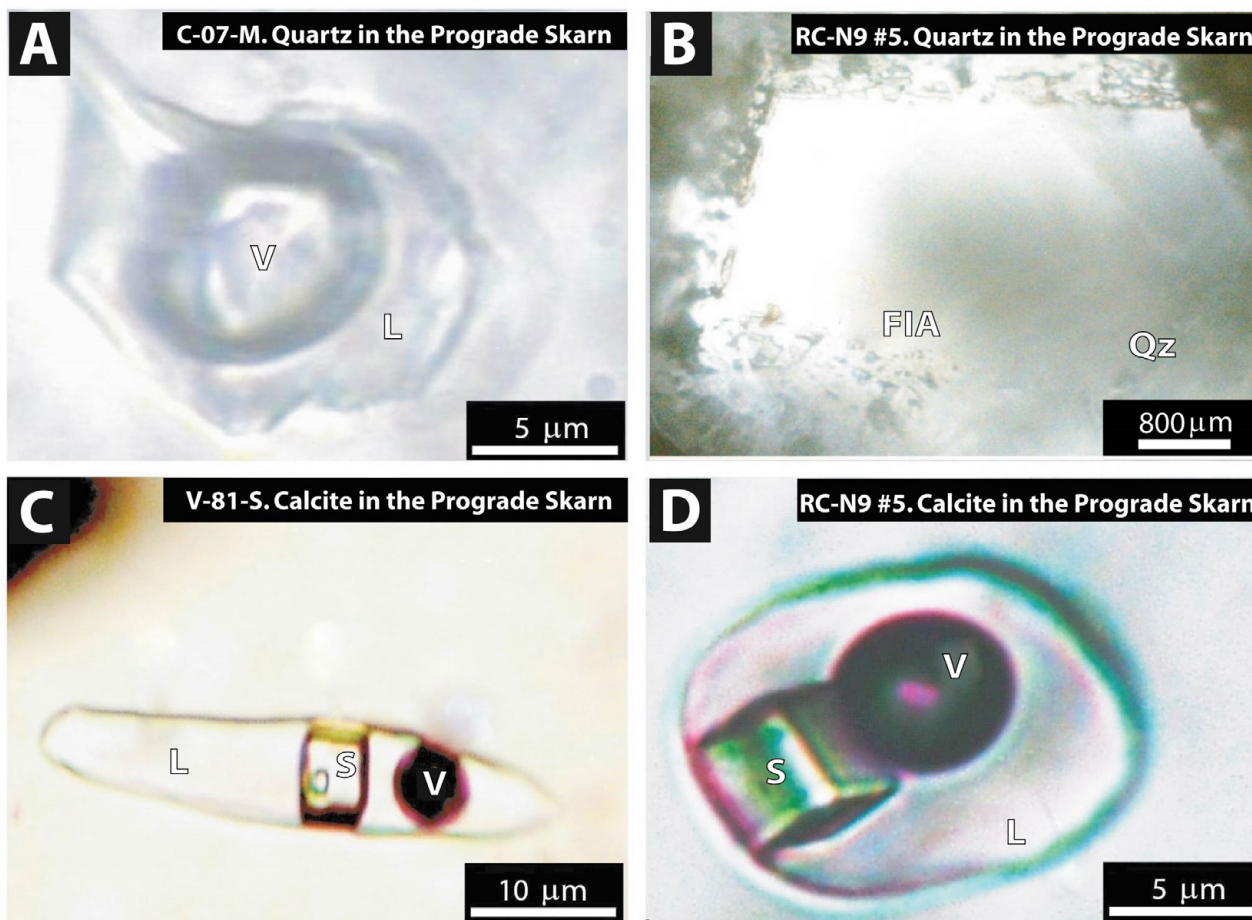
Figure 9 Photomicrographs of fluid inclusions from the Velardeña skarns and veins. (A) liquid + vapor fluid inclusions in quartz (sample C-07-M). (B) FIA (fluid inclusion association) in sample RC-N9 # 5; (C) Fluid inclusion in calcite with liquid (L) + vapor (V) + solid (S) (halite) (sample V-81-S). (D) Fluid inclusion in calcite with liquid + vapor + solid (halite) (sample RC-N9 # 5); Qz: quartz.

generally including a prograde (high temperature) stage and a subsequent retrograde (lower temperature) stage (*e.g.,* Einaudi *et al.*, 1981). The prograde stage is dominated by progressive reactions that produce high temperature minerals, typically calcic garnet and clinopyroxene (*e.g.,* Logan, 2000; Canet *et al.*, 2009, 2011a). In the Velardeña skarns, clinopyroxene has a relict character and occurs as inclusions within poikilitic garnet, which indicates that garnet formed after clinopyroxene (Figures 3a and 4a). Two possible reactions leading garnet formation, regardless of the chemical variability of the calc-silicates involved, are (Figure 12):

2 hedenbergite + calcite + 0.5 O_2 → andradite + quartz + CO_2 (1)

9 hedenbergite + 2 O_2 → 3 andradite + magnetite + 9 quartz (2)
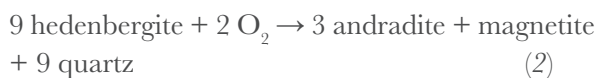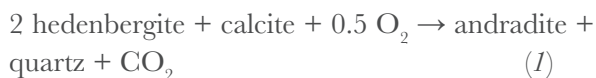
Reaction (1) implies an increase in O_2 fugacity but is little dependent on temperature and is affected by CO_2 fugacity (Bowman, 1998). Besides, it takes place within a relatively narrow range of high temperatures, of ~450–525 °C, which may shift to ~390–490 °C in low $f(CO_2)$ conditions (Figure 12). On the other hand, reaction (2) has a greater dependence on temperature and the minimum temperature at which it can take place drops down to 335 °C (Bowman, 1998) (Figure 10). According to our FI data, the replacement of clinopyroxene by garnet implies a significant decrease of temperature, taking place at ~375 °C, and the T_H range obtained in garnet (337–376 °C) is well below the temperature range for reaction (1), even in low $f(CO_2)$ conditions (Figure 12a). Therefore, reaction (2) better accounts for the evolution of the prograde skarn. The only drawback of this reaction is the absence of magnetite in the studied paragenesis, although this can be explained by (*a*) enhanced $f(O_2)$ conditions, falling up to the stability field of hematite (present in the studied mineral assemblages); and/or (*b*) the low Fe^{2+}/Mg ratio in the clinopyroxene crystals, so they are diopside instead of hedenbergite (Figure 7d).
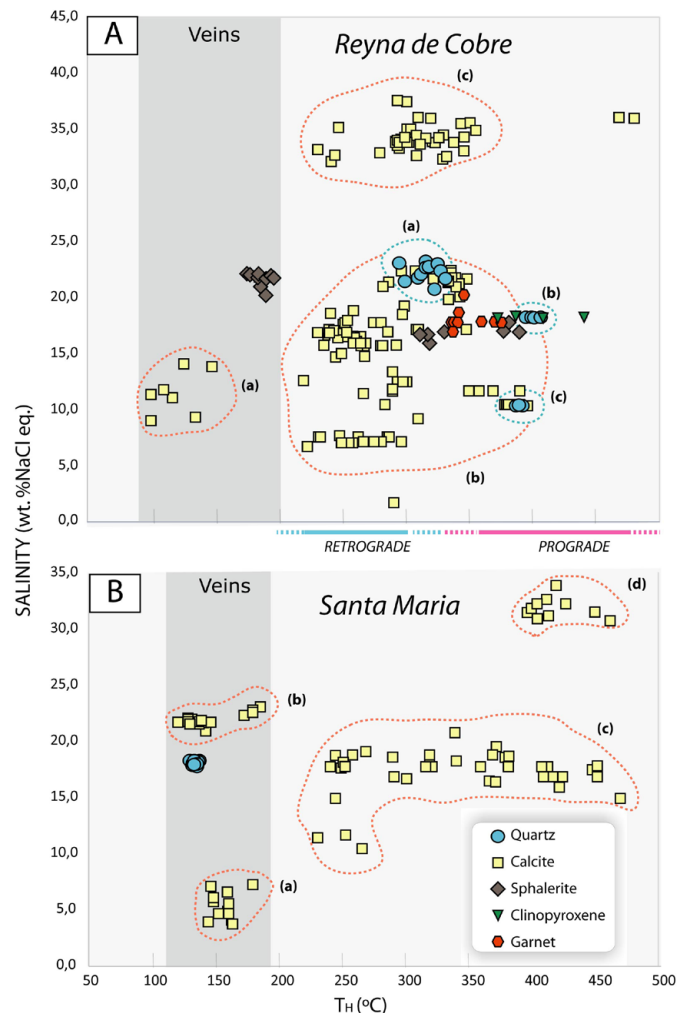
Figure 10 Diagram showing salinity (wt.% NaCl eq.) vs. homogenization temperatures (TH) of the individual fluid inclusions analyzed in the Velardeña skarn and vein deposits (Table 2). (A) FIAs from The Reyna de Cobre deposit. (B) FIAs from Santa Maria Deposit. The assignment of the analyzed minerals to skarn formation stages is shown in Figures 6 and 12.

Wollastonite is another mineral of the prograde stage of the Velardeña skarns, occurring both in the endoskarn and in the exoskarn. Its temperature of crystallization strongly depends on CO_2 partial pressure, being of at least 540 °C with high $f(CO_2)$ or about 475 °C low at low $f(CO_2)$ conditions (Bowman, 1998). Therefore, wollastonite may have been the first-appearing mineral phase of the skarn, having formed during or shortly after the intrusion of granitic magmas into the carbonate rocks, through a reaction that involves calcite
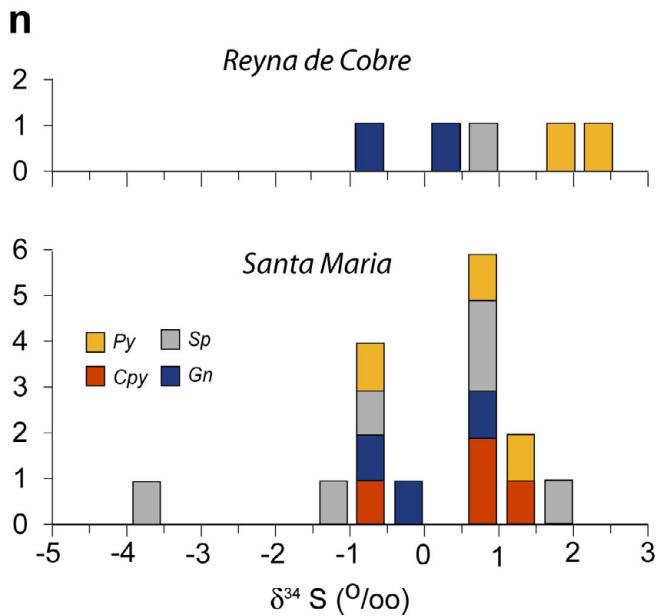
Figure 11 Histograms showing δ^{34}SCDT (in ‰) values of sulfides from the Velardeña skarns and vein deposits (Table 6). (Top) Values from Reyna de Cobre samples. (Bottom) Values from Santa María samples. Py: pyrite, Sp: sphalerite; Cpy: chalcopyrite; Gn: galena.

and quartz and that is independent from $f(O_2)$ (Bowman, 1998; Figure 12a):

$$calcite + quartz \rightarrow wollastonite + CO_2 \qquad (3)$$

Our microthermometry analysis revealed that in the skarns of Velardeña calcite formed in a wide range of temperature conditions (corresponding, therefore, to different FIAs), with T_H reaching values as high as ~470 °C (Table 5), just below the univariant line of reaction (3) at low $f(CO_2)$ conditions (Figure 12b). Besides calcite, quartz formed at high temperature (T_H: 390–400 °C), therefore during the prograde stage (Table 5; Figure 10).

Retrograde assemblages in Zn skarn deposits essentially consist of hydrous silicates(commonly epidote, calcic amphiboles, and chlorite) accompanied by quartz and calcite, and by base metal sulfides (*e.g.*, Einaudi *et al.* 1981; Canet *et al.*, 2009, 2011a). The petrography and SEM study of the Velardeña skarns confirmed the above mineralogy for the retrograde stage, finding also hematite and scheelite, and revealing the pseudomorphic alteration of garnet.

This mineral replacement could be explained by the following reaction (Figure 12):

$$andradite + 3\ CO_2 \rightarrow 3\ quartz + 3\ calcite + hematite \qquad (4)$$
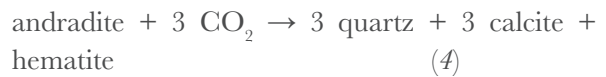
This reaction is independent of the $f(O_2)$ and takes place at 390 °C and high $f(CO_2)$ or at 335 °C and low $f(CO_2)$ (Bowman, 1998; Figure 12c); taking into account that calcic garnets in Velardeña formed at temperatures (T_H) down to 337 °C, the later conditions account for the replacement of garnets and, therefore, the temperature boundary between prograde and retrograde stages should be at ~335 °C (figures 10 and 12). It is noteworthy that most T_H values obtained from FI in calcite and quartz are lower than 335 °C, indicating that these minerals were formed in large amounts when the temperature dropped below this limit (Figure 10). Regarding the sulfides, iron-rich sphalerite (*Sp-1*) was deposited around this temperature limit, according to the T_H measurements (average: 345 °C; Table 5), as well as galena and pyrite, with isotopic (sulfur) equilibrium temperatures of 346 °C.

On the other hand, the lower temperature limit of the retrograde stage could be around 220 °C (Figure 12d), according to the lowest T_H values obtained from calcite other than that from veins (Figure 10).

Accompanying the temperature decline involved in the evolution of the paragenesis of the Velardeña skarns, from over 475 °C to ~220 °C (which comprises the prograde and retrograde stages), there is a general increase in $f(O_2)$ (Figure 12). These changes can be explained by mixing with cooler, oxidizing and dilute water (cf. Hedenquist and Henley, 1985; Wilkinson, 2001; Canet *et al.*, 2011b).

Veins rich in calcite, fluorite, quartz and adularia are found both in Santa María and Reyna de Cobre mineralized areas. These mineralized structures are similar to the typical Mexican low-sulfidation epithermal deposits (cf. Camprubí and Albinson, 2007) and show conditions of formation that are contrasting with those of skarns,

remarkably (*a*) temperatures (T$_H$) below 200 °C; (*b*) high CO$_2$ pressure, revealed by the formation of clathrates during the freezing of FI; and (*c*) strong variations in salinity (in FI), from 7 to 23% NaCl eq. (figures 9b, 9c, and 9d). This variation in salinity (FIA "*d*" in Santa Maria and "*c*" in Reyna de Cobre), along with the occurrence of adularia indicates that boiling affected the hydrothermal system (Figure 10), probably controlling metal deposition (cf. Canet *et al.*, 2011b; Cruz-Pérez *et al.*, 2016).With respect to the isotopic composition of sulfur, differences between skarn and vein mineralizations were found too. The general range of variation of δ^{34}S in sulfides from the skarns, between -1.1 and +2.6‰ (Table 6), unequivocally indicates a magmatic origin for sulfur (Ohmoto and Rye, 1979). Gilmer *et al.* (1988) reported δ^{34}S values from -3.5‰ to 2.5‰ from Santa María, roughly overlapping the results in this study.

In Reyna de Cobre, δ^{34}S values follow the order pyrite > sphalerite > galena (Figure 11), which agrees with the different ^{34}S fractionation factors between these minerals and H$_2$S (Ohmoto and Rye, 1979). In Santa María, where the number of analyses is much higher, no regularity is observed in the distribution of δ^{34}S values per mineral (Figure 11), likely reflecting the effects of differences among stages of mineralization.

On the other hand, the only vein sulfide analysis corresponds to a sphalerite grain (from Santa María) that gave us the lowest δ^{34}S value, of -3.9‰. This ^{34}S depletion relative to the skarn sulfides may account for higher *f* (O$_2$) conditions in the vein mineralizing fluid (which sulfate–sulfide fractionation is significant) even starting from an equal total sulfur isotopic composition, which would correspond, in both cases, to a magmatic source (cf. Ohmoto and Rye, 1979).
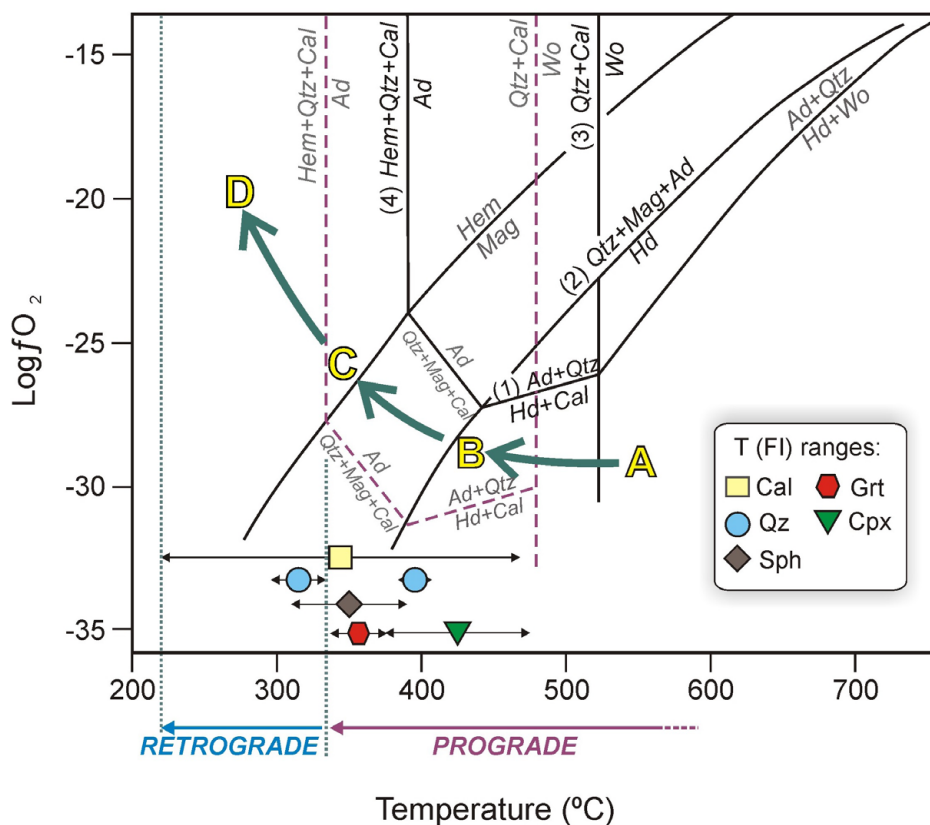
Figure 12 Temperature vs. O2 fugacity diagram (Ca-Fe-Si-C-O-H system at 500 kbar; after Bowman 1998) showing suggested general paths for prograde (A, B, and C) and retrograde (D) stages of formation of the Velardeña skarns. Dashed lines: univariant curves at *f* (CO$_2$) of 1.5 MPa; solid lines: univariant curves at *f* (CO$_2$) of 6 MPa. Mineral abbreviations: Ad: andradite; Cal: calcite; Cpx: clinopyroxene (diopside); Grt: garnet (andradite); Hem: hematite; Hd: hedenbergite; Mag: magnetite; Qz: quartz; Sph: sphalerite; Wo: wollastonite.

Significant differences in ore characteristics, particularly in sphalerite (Fe content, isotopic values and T_H) between the skarn (prograde and retrograde stages) and the epithermal veins suggest an overprinting process. Normal faulting should have allowed veins formed at high crustal levels to overprint the deeper and earlier skarn deposits, resulting in a telescoped mineral system (cf. Sillitoe, 1994). Moreover, Camprubí (2013) mentioned several other telescoping processes in the Mexican metallogenetic history, not only for skarns (*e.g.*, Cosalá, Sinaloa), but also in other epithermal deposits (Ixtacamaxtitlán, Puebla). According to this, telescoped deposits in the Mexican context are typically polymetallic and/or Ag-rich, and some are overprinting skarn and/or porphyry-type ores, whether they are stacked or telescoped.

6. Concluding remarks

The two skarn occurrences, Reyna de Cobre and Santa María, are very similar in (*a*) structure, composition and paragenesis of the orebodies; (*b*) conditions and evolution of mineralizing fluids; and (*c*) source of sulfur. Therefore, the prospective Reyna de Cobre skarns could be comparable as well in terms of economic potential with Santa María mine, which historically was one of the most productive in central-northern Mexico.

The two skarn occurrences of Velardeña are zinc skarns, formed at hypabyssal depths in the crust (P = 0.8–0.9 kbar; equivalent to 3–4 km depth) along the intrusive contact between Cretaceous limestones and Oligocene stocks and dikes of granitic to granodioritic composition.

These skarns formed by a succession of replacive mineralizing events, including a prograde stage and a subsequent retrograde stage. The prograde stage is characterized by the formation of wollastonite, andradite and diopside, along with calcite and minor quartz. This stage took place at temperatures from ≥470 °C to 335 °C, in conditions of low f (CO_2). The retrograde stage produced actinolite, clinozoisite and chlorite accompanied by abundant quartz and calcite, along with subordinate hematite, scheelite and sulfides (pyrite, arsenopyrite, sphalerite, galena, chalcopyrite and pyrrhotite), and sulfosalts (lillianite and boulangerite). This stage took place from 335 °C until temperature dropped to 220 °C. Accompanying the temperature decline involved in the formation of the skarns, there is a general increase in f (O_2), which accounts for a process of mixing with cooler, oxidizing and dilute water.

Epithermal veins with calcite, sphalerite, fluorite, quartz and adularia are found in both study areas, showing conditions of formation that are contrasting with those of the skarns; they constitute on the whole a telescoped skarn–epithermal mineral system. The source of sulfur is purely magmatic for both skarn and epithermal mineralization.

Acknowledgements

References

Aguirre-Díaz, G. J., Labarthe-Hernández, G., Tristán-González, M., Nieto-Obregón, J., Gutiérrez-Palomares, I., 2008, Ignimbrite Flare-up and graben-calderas of the Sierra Madre Occidental, Mexico, in Gottsmann, J., Martí, J. (eds.), Caldera Volcanism: Analysis, Modelling and Response, Developments in Volcanology 10: Amsterdam, Elsevier,

REFERENCES

143-180. https://doi.org/10.1016/s1871-644x(07)00004-6

Ambriz, M. D., 1979, Geología y yacimientos minerales de la mina Santa María, en Velardeña, Dgo. (abstract), in XIII Convención Nacional de la Asociación de Ingenieros de Minas, Metalurgistas y Geólogos de México, 225-260.

Barboza-Gudiño, J. R., Tristán-González, M., Torres-Hernández, J. R., 1998, The late Triassic-early Jurassic active continental margin of western north America in northeastern Mexico: Geofísica Internacional, 37, 283-292.

Barboza-Gudiño, J. R., Hoppe, M., Gómez-Anguiano, M., Martínez-Macías, P. R., 2004, Aportaciones para la interpretación estratigráfica y estructural de la porción noroccidental de la Sierra de Catorce, San Luis Potosí, México: Revista Mexicana de Ciencias Geológicas, 21, 299-319.

Bodnar, J., Reynolds, J., Kuehn, C. A., 1985, Fluid inclusion systematics in epithermal systems: Review in Economic Geology, 2, 73-96.

Bodnar, R. J., Vityk, M. O., 1994, Interpretation of microthermometric data for H_2O-NaCl fluid inclusions, in De-Vivo, B., Frezzotti M. L. (Eds.), Fluid inclusions in minerals: Methods and applications: U.S.A., Virginia Polytechnic Institute and State University, 117-130.

Bowman, J. R., 1998, Basic aspects and applications of phase equilibria in the analysis of metasomatic Ca-Mg-Al-Fe-Si skarns, in Lentz, D.R. (ed.), Mineralized intrusions–related skarns systems: Quebec, Mineral Association of Canada 26, 359-414.

Camprubí, A., 2009, Major metallogenic provinces and epochs of Mexico: SGA News, 25, 1-20.

Camprubí, A., 2013, Tectonic and Metallogenietic History of Mexico: Chapter 6 Society of Economic Geologists, Special Publication, 17, 201-243.

Camprubí, A., Albinson, T., 2007, Epithermal deposits in Méexico — update of current knowledge, and an empirical

reclassification: Geological Society of America Special Paper, 377-416. https://doi.org/10.1130/2007.2422(14)

Canet, C., Camprubí, A., González-Partida, E., Linares, C., Alfonso, P., Piñeiro-Fernández, F., Prol-Ledesma, R. M., 2009, Mineral assemblages of the Francisco I. Madero Zn-Cu-Pb-(Ag) deposit, Zacatecas, Meéxico: implications for ore deposit genesis: Ore Geology Reviews, 35 (3-4), 423-435. https://doi.org/10.1016/j.oregeorev.2009.02.004

Canet, C., González-Partida, E., Camprubí, A., Castro-Mora, J., Romero, F. M., Prol-Ledesma, R. M., Linares, C., Romero-Guadarrama, J. A., Sánchez-Vargas, L. I., 2011a, The Zn-Pb-Ag skarns of Zacatepec, Northeastern Oaxaca, México: A study of mineral assemblages and ore forming fluids: Ore Geology Reviews, 39 (4), 277-290. https://doi.org/10.1016/j.oregeorev.2011.03.007

Canet, C., Franco, S. I., Prol-Ledesma, R. M., González-Partida, E., Villanueva-Estrada, R. E., 2011b, A model of boiling for fluid inclusion studies: Application to the Bolaños Ag-Au-Pb-Zn epithermal deposit, Western Mexico: Journal of Geochemistry Exploration, 110(2), 118-125. https://doi.org/10.1016/j.gexplo.2011.04.005

Clark, K. F., Foster, C. T., Damon, P. E., 1982, Cenozoic mineral deposits and subduction-related magmatic arcs in Meéxico: Geological Society of America Bulletin, 93 (6), 533-544. https://doi.org/10.1130/0016-7606(1982)93<533:cmdasm>2.0.co;2

Cruz-Pérez, M. A., Canet, C., Franco, S. I., Camprubí, A., González-Partida, E., Rajabi, A., 2016, Boiling and depth calculations in active and fossil hydrothermal systems: A comparative approach based on fluid inclusion case studies from Mexico: Ore Geology Reviews, 72, 603-611. https://doi.org/10.1016/j.oregeorev.2015.08.016

Dal-Negro, A., De-Pieri, R., Quareni, S., Taylor, W. H., 1978, The crystal structures of nine

K feldspars from the Adamello Massif (Northern Italy): Acta Crystallographica Section B, 34 (9), 2699-2707. https://doi.org/10.1107/s056774087800905x

Damon, P., Shafaullah, M., Clark, K., 1981, Evolución de los arcos magmáticos de México y su relación con la metalogénesis: Revista Mexicana de Ciencias Geológicas, 5, 223-238.

Eguiluz-De-Antuñano, S., Aranda-García, M., Marrett, R., 2000, Tectónica de la Sierra Madre Oriental,. México: Boletín de la Sociedad Geológica Mexicana, 53 (1), 1-26. https://doi.org/10.18268/bsgm2000v53n1a1

Einaudi, M. T., Meinert, L. D., Newberry, R. J., 1981, Skarn deposits: Economic Geology 75th Anniversary Volume, 317–391.

Felder, F., 1979, Estudio de algunas estructuras mineralizadas en el domo de Santa María Velardeña, Dgo. (abstract), in XIII Convención Nacional de la Asociación de Ingenieros de Minas, Metalurgistas y Geólogos de México, 192-224.

Ferrari, L., Valencia-Moreno, M., Bryan, S., 2005, Magmatismo y tectónica en la Sierra Madre Occidental y su relación con la evolución de la margen occidental de Norteamérica: Boletín de la Sociedad Geológica Mexicana, 57, 343-378. https://doi.org/10.18268/bsgm2005v57n3a5

Gilmer, A. L., Clark, F., Hernandez, C. I., Conde, C. J., Figueroa, S. J. I., 1986, Geological and mineralogical summary of the metalliferous deposits in the Santa María dome, Velardeña, Durango, in Clark, F., Megaw, P. K., Ruiz, J. (eds.), Lead-zinc-silver carbonate hosted deposits of Northern Mexico: Society of Economic Geology, 143-153.

Gilmer, A. L., 1987a, The geology and genesis of the Sierra de Santa María metalliferous deposits, Velardeña, Durango, Mexico: University of Texas, MSc thesis, 349 p.

Gilmer, A. L., 1987b, Tectonic controls on carbonate-replacement mineralization in the northern Mexican province: U.S.A., Department Colloquium of the University of Texas 61-82.

Gilmer, A. L., Clark, K. F., Conde, C. J., Hernandez, C. I., Figueroa, S. J. I., Porter, E. W., 1988, Sierra de Santa Maria, Velardena mining district, Durango: Economic Geology, 8, 1802-1829. https://doi.org/10.2113/gsecongeo.83.8.1802

Hawthorne, F. C., Oberti, R., Harlow, G. E., Maresch, W. V., Martin, R. F., Schumacher, J. C., Welch, M. D., 2012, IMA Report: Nomenclature of the amphibole supergroup: American Mineralogist, 97, 2031-2048.

Hedenquist, J., Henley, R., 1985, The importance of CO_2 on freezing point measurements of fluids inclusions: evidence from active geothermal systems and implications for epithermal ore deposition: Economic Geology, 80 (5), 1379-1406. https://doi.org/10.2113/gsecongeo.80.5.1379

Hutchinson, M.N., Scott, S. D., 1981, Sphalerite geobarometry in the Cu–Fe–Zn–S system: Economic Geology, 76 (1), 143-153. https://doi.org/10.2113/gsecongeo.76.1.143

Industrias Peñoles, 2016, updated 01/01/2016, http://www.penoles.com.mx/, accessed 26/01/2016.

Jiménez-Franco, A., 2012, Estudio de la paragénesis, inclusiones fluidas e isotopía del azufre del skarn de Velardeña, Durango, Mexico, Posgrado en Ciencias de la Tierra, Universidad Nacional Autónoma de México, MSc thesis, 81 p.

Kelly, W. A., 1936, Evolution of the Coahuila Peninsula, Mexico, Part II, geology of the mountains bordering the valley of Acatita and las Delicias: American Association of Petroleum Geologists, 47, 1009-1038.

Leake, B. E., Woolley, A. R., Birch, W. D., Burke, E. A., Ferraris, G., Grice, J. D., Hawthorne, F. C., Kisch, H. J., Krivovichev, V. G., Schumacher, J. C., Stephenson, N. C. N., Whittaker, E. J. W., 2004, Nomenclature of amphiboles: additions and revisions to the

REFERENCES

The Velardeña Zn-(Pb–Cu) skarn-epithermal deposits, central-northern Mexico

International Mineralogical Association's amphibole nomenclature: Mineralogical Magazine, 68 (1), 209-215. https://doi.org/10.1180/0026461046810182

Levich, A., 1973, Geology and ore deposits of the Sierra de Santa Maríía, Velardeña, Durango, Mexico: University of Texas, MSc thesis,148.

Logan, M. A. V., 2000, Mineralogy and geochemistry of the Gualilán skarn deposit in the Precordillera of western Argentina: Ore Geology Reviews, 17 (1-2), 113-138. https://doi.org/10.1016/s0169-1368(00)00009-3

Lusk, J., Scott, S. D., Ford, C. E., 1993, Phase relations in the Fe-Zn-S system to 5 kbars and temperatures between 325 degrees and 150 degrees C: Economic Geology, 88 (7), 1880-1903. https://doi.org/10.2113/gsecongeo.88.7.1880

Meinert, L. D., Dipple, G. M., Nicolescu, S., 2005, World Skarn Deposits: Economic Geology 100th Anniversary Volume, 299-336.

Morimoto, N., Fabries., J., Fergusson, A. K., Ginzburg, I. V., Ross, M., Seifert, F. A., Zussman, J., Aoki, K., Gottard, G., 1988, Nomenclature of pyroxenes: American Mineralogist, 73, 1123-1133.

Nieto-Samaniego, A. F., Alaniz-Alvarez, S., Camprubí, A., 2005, La Mesa Central de México: estratigrafía, estructura y evolución tectónica cenozoica: Boletín de la Sociedad Geológica Mexicana, 57 (3), 285-318. https://doi.org/10.18268/bsgm2005v57n3a3

Ohmoto, H., Rye, R. O., 1979, Isotopes of sulfur and carbon, in Barnes, H. L., (ed.), Geochemistry of Hydrothermal Ore Deposits 2nd ed.: New York, Willey, 509-567.

Pinet, N., Tremblay, A., 2009, Structural analysis of the Velardeña mining district, Mexico: a faulted Au-Ag-rich hydrothermal system: Canadian Journal of Earth Sciences, 46 (2), 123-138. https://doi.org/10.1139/e09-007

Roedder, E., 1984, Fluid inclusions, in Ribbe, P.H. (ed.), Reviews in Mineralogy: U.S.A.,

Mineralogical Society of America, 79-108.

Rogers, C. L., de-Cserna, Z., Van-Vloten, R., Tavera-Amezcua, E., Ojeda-Rivera, J., 1961, Reconocimiento geológico y depósito de fosfato del norte de Zacatecas y áreas adyacentes en Coahuila, Nuevo León y San Luis Potosí: Boletín del Consejo de Recursos Naturales No Renovables, 56, 1-332.

Sociedad Geológica Mexicana (SGM), 1997, Carta geológico-minera Velardeña G13-D44, 1:50,000: Durango, México, Servicio Geológico Mexicano, 1 map with text.

Sociedad Geológica Mexicana (SGM), 2014, Panorama minero del estado de Zacatecas: Servicio Geológico Mexicano, 61 p.

Shimazaki, H., 1975, The Ratios of Cu/Zn-Pb of Pyrometasomatic Deposits in Japan and Their gGenetical Implication: Economic Geology, 4, 717-724. https://doi.org/10.2113/gsecongeo.70.4.717

Sillitoe, R. H., 1994, Erosion and collapse of volcanoes; Causes of telescoping in intrusion-centered ore deposits: Geology, 22 (10), 945-948. https://doi.org/10.1130/0091-7613(1994)022<0945:eacovc>2.3.co;2

Southern Copper Corporation, 2016, Operaciones Integradas, updated 01/01/2016, available <http://www.southerncoppercorporation.com/ENG/intope/Pages/PGIntOperation.aspx#cuadros>, accessed 01/25/2016.

Spurr, J. E., Garrey, G. H., 1908, Ore deposits of the Velardeña district, México: Economic Geology, 3 (8), 688-725. https://doi.org/10.2113/gsecongeo.3.8.688

Van-den-Kerkhof, A. M., Hein, U. F., 2001, Fluid inclusion petrography: Lithos, 55 (1-4), 27-47. https://doi.org/10.1016/s0024-4937(00)00037-2

Wilkinson, J. J., 2001, Fluid inclusions in hydrothermal ore deposits: Lithos, 55, 229-272. https://doi.org/10.1016/s0024-4937(00)00047-5